The sediment green-blue color ratio as a proxy for biogenic silica productivity along the Chilean Margin.

Chen Li[1], Vincent J Clementi[2], Samantha Claudia Bova[2], Yair Rosenthal[3], Laurel B Childress[4], James Wright[2], and Zhimin Jian[5]

[1]Tongji University
[2]Rutgers University
[3]Rutgers, The State University of New Jersey
[4]International Ocean Discovery Program, Texas A&M University
[5]State Key Laboratory of Marine Geology, Tongji University

November 26, 2022

Abstract

Sediment cores recently collected from the Chilean Margin during D/V *JOIDES Resolution* Expedition 379T (JR100) document high- and low-frequency variability in shipboard-generated records of the spectral Green/Blue (G/B) ratio. These changes show a strong coherence with foraminiferal isotope composition, Antarctic ice core records, and sediment lithology (e.g., higher diatom abundances in greener sediment intervals), suggesting a climate-related control on the G/B ratio. Here, we test the utility of G/B as a proxy for diatom productivity at Sites J1002 and J1007 by calibrating G/B to measured biogenic opal. Strong exponential correlations between measured opal content and the G/B ratio were found at both sites. We use the empirical regressions to generate continuous records of opal contents (opal%) on the Chilean Margin. Redox-sensitive sedimentary U/Th generally co-varies with the reconstructed opal% at both sites, supporting the association between sediment color, sedimentary U/Th, and productivity. Lastly, we calculated opal mass accumulation rate (MAR) at Site J1007 over the last ~150,000 years. The G/B-derived opal MAR record from Site J1007 largely tracks existing records derived from traditional wet-alkaline digestion from the south and eastern equatorial Pacific Ocean, with a common opal flux peak at ~ 50 ka suggesting that this increased diatom productivity in the eastern equatorial Pacific was likely driven by enhance nutrient supply from the Southern Ocean rather than dust inputs as previously suggested. Collectively, our results identify the G/B ratio as a useful tool with the potential to generate reliable, high-resolution paleoceanographic records that circumvent the traditionally laborious methodology.

The sediment green-blue color ratio as a proxy for biogenic silica productivity along the Chilean Margin.

Chen Li[1,2]*, Vincent J. Clementi[1]*, Samantha C. Bova[1,3], Yair Rosenthal[1,4], Laurel B. Childress[5], James D. Wright[4], Zhimin Jian[2], and Expedition 379T Scientists[†]

[1]Department of Marine and Coastal Sciences, Rutgers University, New Brunswick, New Jersey, USA
[2]State Key Laboratory of Marine Geology, Tongji University, Shanghai, China
[3]Present address: Department of Geological Sciences, San Diego State University, San Diego, California, USA
[4]Department of Earth and Planetary Sciences, Rutgers University, New Brunswick, New Jersey, USA
[5]International Ocean Discovery Program, Texas A&M University, College Station, Texas, USA

[†]A list of authors and affiliations appears at the end of the paper

Corresponding authors: Chen Li (1532983@tongji.edu.cn), Vincent J. Clementi (clementi@marine.rutgers.edu)
*These authors contributed equally to this work.

Key Points:

1. Sediment green-to-blue ratio serves as a novel proxy for changes in diatom productivity on the Chilean Margin.
2. Continuous opal percent and opal mass accumulation rates derived from sediment green-to-blue ratio agree with existing records spanning the last 150 kyr but provide greater detail.
3. The sediment green-to-blue ratio proxy is potentially applicable in other regions of high diatom productivity but would require a site-specific calibration.

Abstract

Sediment cores recently collected from the Chilean Margin during D/V *JOIDES Resolution* Expedition 379T (JR100) document high- and low-frequency variability in shipboard-generated records of the spectral Green/Blue (G/B) ratio. These changes show a strong coherence with foraminiferal isotope composition, Antarctic ice core records, and sediment lithology (e.g., higher diatom abundances in greener sediment intervals), suggesting a climate-related control on the G/B ratio. Here, we test the utility of G/B as a proxy for diatom productivity at Sites J1002 and J1007 by calibrating G/B to measured biogenic opal. Strong exponential correlations between measured opal content and the G/B ratio were found at both sites. We use the empirical regressions to generate continuous records of opal contents (opal%) on the Chilean Margin. Redox-sensitive sedimentary U/Th generally co-varies with the reconstructed opal% at both sites, supporting the association between sediment color, sedimentary U/Th, and productivity. Lastly, we calculated opal mass accumulation rate (MAR) at Site J1007 over the last ~150,000 years. The G/B-derived opal MAR record from Site J1007 largely tracks existing records derived from traditional wet-alkaline digestion from the south and eastern equatorial Pacific Ocean, with a common opal flux peak at ~ 50 ka suggesting that this increased diatom productivity in the eastern equatorial Pacific was likely driven by enhance nutrient supply from the Southern Ocean rather than dust inputs as previously suggested. Collectively, our results identify the G/B ratio as a useful tool with the potential to generate reliable, high-resolution paleoceanographic records that circumvent the traditionally laborious methodology.

Plain Language Summary

The color of marine sediments often corresponds to oceanic and sedimentary processes that can influence the global climate system. Visual inspection of new sediment cores collected from the Chilean Margin revealed substantial downcore changes in green and blue sediment colors.

Greener sediment intervals were usually enriched with diatoms, whereas bluer sediments were rich in clay minerals. A specialized camera was used to scan the cores and enable us to quantitatively describe the core colors using the green/blue ratio. The similarity of the downcore green/blue ratio with Antarctic ice core records suggests that it may serve as a quick tool to estimate the age of the cores during the cruise. In this paper, we show that changes in the green/blue ratio are a function of diatom (biogenic opal) productivity and use a calibrated relationship to calculate a continuous record of opal flux at the Chilean Margin over the last 150,000 years. A distinct opal flux maxima at 50,000 years ago is observed, similar to previous studies in the eastern equatorial Pacific. This common event implies a tight link between the high- and low- latitude eastern Pacific Ocean, potentially attributable to enhanced nutrient supply from the Southern Ocean.

1. Introduction

Variations in Southern Ocean and South Pacific primary productivity have been invoked as possible drivers of glacial-interglacial climate change and atmospheric CO_2 variability (Brzezinski et al., 2002; Matsumoto et al., 2002; Sigman & Boyle, 2000; Toggweiler et al., 2006). Our understanding of the role primary productivity plays in the climate system on these timescales is partly attributable to records of opal mass accumulation rates (MAR) in marine sediments (Anderson et al., 2009; Bradtmiller et al., 2007; Charles et al., 1991; Dubois et al., 2010). Many of the records spanning glacial timescales, however, do not have adequate resolution to resolve (sub)millennial-scale changes, which have been shown to influence both the inception and termination of glacial periods (Jouzel et al., 2007). This is partly because the traditional wet-alkaline methods that are used to derive these records are laborious (e.g., Mortlock & Froelich, 1989), which limits the viability of generating continuous, high-resolution records of opal MAR across glacial-interglacial intervals.

One potential avenue to circumvent this obstacle and generate high-resolution opal MAR records is by utilizing the color spectrum of marine sediments derived from core image scanning (Mix et al., 1995; Nederbragt et al., 2000). Generation of sedimentary red-green-blue (RGB) records upon core recovery is standard for most paleoceanographic coring operations and can provide millimeter-scale resolution of sediment properties (e.g., Mix et al., 1992). These data are often translated to L*, a*, and b* values, which have been widely used for core stratigraphy and paleoceanographic reconstructions (e.g., Peterson et al. 2000). However, the raw RGB data may be of equal utility since variations in the sediment color often correspond to key oceanic or sediment processes (e.g., primary productivity, terrigenous input, and sediment diagenesis). For example, Mix et al. (1992) documented a close correlation between high Red/Blue ratios and the presence of sulfides in Eastern Equatorial Pacific (EEP) marine sediment, and Penkrot et al. (2018) reported that the Green/Blue ratio closely tracks biogenic opal in sediment cores taken from the Gulf of Alaska. While these are important observations, the established relationships are qualitative. To leverage these high-resolution records for reconstructing regional primary productivity, an empirical relationship between RGB variables (e.g., Green/Blue) and a lithologic component (e.g., biogenic opal) must be established.

Recent drilling operations on the south Chilean Margin (D/V *JOIDES Resolution* Exp. 379T funded through the NSF *JR100* program) recovered 100-m sediment cores to investigate (sub)millennial-scale to glacial-interglacial variability since the penultimate glaciation. Here, we utilize sites J1002 and J1007 (Figure 1), which document high-frequency changes in the sediment spectral Green/Blue (G/B) ratio. The G/B data were initially used onboard as a stratigraphic tool owing to similarities with global climate records (e.g., EDML ice core). Shipboard lithologic analyses subsequently revealed that sediments enriched with diatoms coincide with high spectral green values, whereas clay-rich sediments corresponded with high blue values. Thus, G/B records in Chilean Margin cores may serve as a paleoceanographic archive of opal percentage in regional sediments.

In this paper, we first explore the conceptual background of the proxy itself, as well as the rationale for using G/B in our stratigraphic efforts. We then test the hypothesis that the G/B record correlates with opal content in sediments on the Chilean Margin by calibrating the proxy to biogenic opal concentrations quantified by traditional methods (Mortlock & Froelich 1989). Lastly, we use the G/B records and initial core stratigraphy based on radiocarbon ages and benthic oxygen isotope records to generate continuous opal MAR records for the last ~150,000 years at Site J1007, offering the highest resolution record of diatom productivity in the south Pacific Ocean through most of the last glacial cycle.

2. Materials and Methods

2.1 Geological and oceanographic settings

Our study region in the southeast Pacific Ocean ranges from the central to south Chilean Margin, where the northward deflection of Antarctic Circumpolar Current (ACC) forms the Peru-Chile Current (PCC, a.k.a Humboldt Current) between 40°S-45°S (Strub et al., 1998). The northward flowing PCC dominates the surface circulation pattern along the west coast of South America

(Figure 1). The poleward flowing Gunther Undercurrent underlies the PCC between 100-400 m water depth (Hebbeln et al., 2000; Strub et al., 1998). Between 500-1200 m water depth flows Antarctic Intermediate Water (AAIW), which forms today at the Subpolar Front by mixing cold, fresh Polar Front waters with Subantarctic Mode Water (Piola and Georgi 1982; Sallée et al. 2010; Sloyan and Rintoul, 2001). Beneath AAIW sits the northern flowing Antarctic Bottom Water and sluggish Pacific Deep Water (PDW) return flow, which enters the Southern Ocean at mid-depths (Talley, 2013). Coastal upwelling is intensive throughout the year north of 35°S but is restricted to late spring and early fall between 35°S-42°S. South of 42°S, coastal upwelling is inhibited by the prevailing southern westerly winds (Strub et al., 1998).

The current oceanographic regime makes the Chilean Margin a remarkably productive region in the modern setting. Annual chlorophyll concentration in surface waters along the Chilean Margin reaches up to 4 mg/m^3 (Figure 1b). Annual primary productivity in this region is dominated by diatoms (Abrantes et al., 2007), and based on satellite-measured pigments is estimated to about ~150 gC/m^2/yr off central Chile (31°S-37°S) and ~60 gC/m^2/yr along the south Chilean Margin (i.e., south of 37°S; Antoine and Morel, 1996). The latitudinal distribution pattern of opal contents (opal%) and organic carbon contents (C_{org}%) in surface sediment samples reflect the overlying pigment concentration; surface sediment opal% ranges from ~5% off central Chile to ~3% in the south (Romero and Hebbeln, 2003). Despite the high diatom productivity in this region, the opal percentages in the sediments are very low because of the extremely high sedimentation rates on the margin, which can exceed 200 cm/kyr (Hebbeln et al., 2007). High sedimentation rates along the Chilean Margin are largely attributable to significant regional precipitation and high elevations of the Coastal Range and the Andes. Precipitation can vary from <1000 mm/yr in central Chile to >2500 mm/yr south of 40°S, leading to increased terrigenous supply in the south (Stuut et al., 2006).

2.2 Study sites

Sites J1002 and J1007 were recovered from the Chilean Margin using the D/V *JOIDES Resolution* drilling platform during Expedition 379T in Summer 2019 (Figure 1). Site J1002 (46° 4.2964′S, 75° 41.2300′W) is located on the south Chilean Margin offshore Northern Patagonia on a bench in the continental slope at a water depth of 1534 m. At present, this site lies under the northern extent of the ACC and is bathed in PDW. Site J1007 (36° 32.5400′S, 73° 39.9900′W) is located on the continental crust 60 km shoreward of the Chile Trench. With a water depth of 808 m, Site J1007 lies in the heart of modern AAIW (Bova et al., 2021).

2.3 Age models

Age models for Site J1002 and J1007 (Figure S2, S3; see age control points in Table S3) were based on a combination of AMS radiocarbon dating and the visual correlation to the LR04 benthic stack (Lisiecki and Raymo, 2005). Calendar ages for the upper parts of the core are based on AMS ^{14}C dating of planktonic foraminifera (*Globigerina bulloides*): eight in the upper 67 m of Site J1002 and seven in the upper 23 m at Site J1007, with calendar corrections using IntCal20 (Reimer et al., 2020; Figure 3). Below these depths, stratigraphy is based on visual correlation between benthic foraminifer *Uvigerina spp.* $\delta^{18}O$ and the LR04 benthic stack. The *Undatable* program has been used to refine the original age models (Lougheed et al., 2019), improving the resolution and precision of the opal flux estimate simultaneously (See age-depth figures in Figure S1). Comparison with benthic $\delta^{18}O$ from the nearby ODP Site 1234 (36°14′S, 73°41′W, 1015 m; de Bar et al., 2018; Heusser et al., 2006; Robinson et al., 2007) is further applied to constrain the J1007 age model. Nonetheless, we note that the J1007 age model below 66 m is loosely constrained due to limited resolution of the benthic $\delta^{18}O$ record. For J1007, the interval between 82 m to 86 m is thought to represent the light $\delta^{18}O$ "plateau" of Marine Isotope Stage (MIS) 5e. However, the $\delta^{18}O$ of this recognized MIS 5e stage are not significantly more depleted than the Holocene as might be expected. Therefore, we caution that it is possible that the real MIS 5e "plateau" was missed due to low sampling resolution and the bottom of J1007 does not reach MIS 5e. This uncertainty has, however, no bearings on the discussion and conclusion of the paper but should be noted by potential users of the core data.

2.4 Spectral G/B ratio

Although extremely high sedimentation rates along the southern Chilean Margin offer the opportunity to generate high-resolution paleoproductivity records, they also pose a few challenges. First, the concentration of biogenic components (e.g., organic carbon% and opal%) are very low, approaching the detection limits of the analytical methods. And secondly, taking advantage of the high sedimentation rates for generation of high-resolution records using traditional methods is laborious and practically unattainable. Therefore, continuous methods can offer valuable information that cannot be obtained from discrete measurements. The advantage of such a method is more in capturing the temporal variability at high resolution than in providing accurate concentrations. The spectral G/B ratio is a quantitative method to describe sediment color in the wavelengths of green and blue ranges. Shipboard color reflectance spectrophotometry was measured on the archive halves of the core using a line-scan camera on the automated Section Half Imaging Logger (SHIL). Sediment cores were scraped using a glass slide after splitting, and the cleaned flat face of the archive half was immediately imaged to prevent color degradation at a resolution of 10 lines/mm. Data were presented as color reflectance parameters of red, green, and blue (Bova et al., 2021). The spectral G/B ratio was calculated as the green parameter divided by the blue parameter.

Preliminary results of the shipboard smear slide description suggest a possible link between sediment color and lithology, in agreement with previous work (e.g., Mix et al. 1992; Mix et al. 1995; Nederbragt et al. 2000; Penkrot et al. 2018). Elevated abundance of diatoms is typically found in greener sedimentary intervals (Figure 2). Similar latitudinal distribution patterns of opal%, C_{org}%, and pigment concentrations suggest that diatoms are the dominant group of primary producers along the Chilean Margin (Abrantes et al., 2007; Romero and Hebbeln, 2003; Stuut et al., 2006). The primary pigments of diatoms are the green chlorophyll-*a* and the blue-green chlorophyll-*c* (Kuczynska et al., 2015; Stauber and Jeffrey et al., 1988). Although chlorophyll can be degraded, most of the breakdown products (e.g., chlorins) are still detectable by regular spectrophotometric methods (Ruess, 2005). Indeed, downcore pigment records have been used to reconstruct productivity changes in lakes and estuaries for decades (Ruess et al., 2005; Ruess et al., 2013). Thus, it has been hypothesized that the spectral color of green is mainly produced by diatom-related pigments in this region. In contrast, cores with a dominance of siliciclastic components and a lower abundance of diatoms are usually found to be bluer (Figure 2). Considering the tremendous terrestrial input commonly found along the Chilean Margin, the siliciclastic component likely produces the blue spectral color. We therefore hypothesize that the spectral G/B ratio reflects the relative abundance of biogenic silica in sediments, and based on our calibration, can use it as to quantify diatom productivity along the Chilean Margin over time.

Given the high-temporal variability of the records, the spectral G/B ratio has also been a useful tool for stratigraphic correlations among holes drilled during Expedition 379T because it is likely linked to regional climate processes (Bova et al., 2021). Previous studies suggest that Antarctic climate changes have a significant impact on surface water dynamics and terrestrial input off of the coast of Chile (Lamy et al., 2004; Kaiser et al., 2007). Regional surface water processes are closely linked to diatom production, hence the spectral green parameter of the sediments. On the other hand, the terrestrial input is assumed to contribute to the spectral blue parameter in sediments. The variation of spectral G/B ratio may be sensitive to climate dynamics, making it applicable for stratigraphic correlations. To validate these assumptions, we compare the downcore variations in G/B at J1002 and J1007 with the benthic foraminiferal $\delta^{18}O$ record at each site. The remarkable consistency between the G/B and benthic $\delta^{18}O$ at both sites validates the use of the G/B ratio for stratigraphic correlations along the Chilean Margin (Figure 3). Moreover, G/B ratios at both sites show good correlations with Antarctic ice core $\delta^{18}O$ records, with higher G/B values usually corresponding to warm intervals near Antarctica and lower G/B values corresponding with cold intervals; this observation further demonstrates its utility for stratigraphic correlations (Figure 3). This tool has been especially useful for shipboard correlation as other sedimentary property records in these regions (e.g., magnetic susceptibility, natural gamma radiation, and other color properties) had muted signals. For example, magnetic susceptibility was widely used for shipboard correlation among holes, but for high sedimentation rate sites—especially those with thick Holocene section that were devoid of any appreciable magnetic susceptibility signal—G/B ratios turned out to be the most applicable stratigraphy tool (Bova et al., 2021).

2.5 Biogenic opal analyses

J1002 and J1007 were sampled at intervals spanning the range of G/B values measured at each site to investigate the relationship between opal% and G/B. Biogenic silica concentrations were measured by conventional wet-alkaline digestion, including mineral correction procedures modified after Conley et al. (2001). The mineral correction was critical for sediments with relatively low biogenic silica contents as it minimizes the effect of mineral silicates. A total of 22 samples from J1002 and 41 samples from J1007 were analyzed. About 250 mg of freeze-dried sediments were homogenized using a mortar and pestle and digested by 1 mol/L Na_2CO_3 solution in an 80°C water bath. The tubes were shaken quickly for complete digestion every 20 minutes. Subsamples of 1 mL were taken after 3, 4, and 5 hours of digestion time. Silicate concentration of each subsample was measured by molybdate blue spectrophotometric measurements using an Agilent Cary 60 UV-Vis Spectrophotometer at Rutgers University peaked at 812 nm, modified after Mortlock and Froelich (1989) (see detailed experimental and data-processing procedure in Text S1). Ideally, a linear regression was made with the three subsamples, with extrapolation to the intercept providing the final biogenic silica concentration (DeMaster, 1979). Finally, opal% was calculated as biogenic silica concentration multiplied by 2.4 (Mortlock and Froelich, 1989). The standard error of our measurements was 0.35% based on 14 duplicate measurements. Wet-alkaline digestion could be affected by "noise" from clay (Conley et al., 2001). Our mineral correction protocol suggests, however, that clay only contributes to a stable background noise of 0.3% (Figure S1), which was then removed during the data-processing procedure.

2.6 Quantifying U and Th contents with shipboard natural gamma radiation data

Full natural gamma radiation (NGR) data for Site J1002 and J1007 were collected during Expedition 379T. Original NGR spectra obtained on board were composed of numerous peaks for the ^{238}U and ^{232}Th series. Thus, sedimentary contents of thorium (^{232}Th), and uranium (^{238}U) were estimated by identifying and quantifying their characteristic energy peaks using a MATLAB algorithm by De Vleeschouwer et al. (2017).

3. Results and Discussions

3.1 Calibration of spectral G/B with measured opal%

Shipboard spectral G/B records exhibit a generally northward increasing trend along the Chilean Margin, in agreement with annual chlorophyll distribution in surface waters (Figure 1b). In addition to lower average values, the G/B for Site J1002 also shows smaller variabilities than J1007. Measured opal% for Site J1002 and Site J1007 vary between 0.36-4.36% and 1.89-5.35%, respectively. In general, measured opal% covary with the G/B, with higher measured opal% usually found in greener sediments (Figure 4a). Eight samples from J1007 and one sample from J1002, however, apparently underestimate opal% with respect to G/B (Table S2). In all cases these intervals are associated with prominent low values of magnetic susceptibility (Figure 5), which hints to the possibility of diagenetic overprints.

At Site J1007, the organic carbon percentage (C_{org}%) correlates well with measured opal% (n=21, r^2=0.51, $p<0.05$; Figure 4b), in agreement with the robust correlation between opal% and C_{org}% in the nearby surface sediments (Romero and Hebbeln, 2003). Those samples with potentially underestimated opal%, within low magnetic susceptibility intervals, are similarly offset from the expected values based on average correlation between opal% and C_{org}%. Preliminary shipboard analysis shows the frequent presence of nannofossils and diatoms in sediments along the Chilean Margin (Bova et al., 2021). Combining downcore and surface sediment records, it can be deduced that primary productivity in this area is dominated by diatomaceous species, with carbonate nannofossil species as a minor contributor. In contrast, C_{org}% shows only a weak correlation with G/B (Figure 4c), which suggests one or both indicators are impacted by degradation. As most degradation products of chlorophyll retain their original color (Ruess, 2005), it is likely the G/B proxy is a more robust indicator and possibly independent of organic matter preservation. Nonetheless, with these caveats in mind, data from low magnetic susceptibly intervals should be considered with higher uncertainty.

Excluding the underestimated data points (20% of entire data set, shown in figure 5), strong exponential correlations are found between G/B and measured opal% at both sites (J1002: $\ln(y)=5.8x-6.3$, n=14, r^2=0.73, $p<0.05$; J1007: $\ln(y)=5.8x-5.5$, n=22, r^2=0.48, $p<0.05$; where x and y are G/B values and opal%; Figure 4a). The calibrations of J1002 and J1007 show the same slope but different intercept, indicating similar sensitivity of G/B and differences in background colors. Root mean square deviation (RMSD) were calculated based on the differences between measured opal% and the reconstructed opal% derived from G/B values. The RMSD is 0.68% for J1002 and 0.72% for J1007, reflecting the uncertainty of regression models in this study.

Note that while the relationships between G/B, opal%, and C_{org}% are robust, the empirical calibrations are site-specific to J1002 and J1007 and cannot be transferred to other sites, even those in the same region. We hypothesize that variable clay mineralogies along the meridional transect (e.g., Lamy et al., 1998) cause spatial differences in the total "blue" content in the sediments, which were presented by different intercepts of the calibration equations. Similar to X-ray fluorescence (XRF) scanning records of cores, the G/B ratio may also provide a semi-quantitative record that will require a site-specific calibration at each site to convert the relative changes to a record of opal%. It is noteworthy, however, that the two studied sites represent an extreme case where the opal concentrations are very low due to dilution from the very high sedimentation rates. It is likely that the method and calibration would be more robust in sites where the contribution of clays and sedimentation rates are lower than those encountered on the Chilean Margin.

3.2 Reconstructing opal% records

Having established the G/B proxy as a tracer of opal% at our study sites, we now use the exponential regression equations above to reconstruct past changes of opal% from the G/B records. Downcore opal% ranges between 0.6-2.5% and 1.6-8.8% for J1002 and J1007, respectively (Figure 5). Reconstructed opal% shows relatively large-scale variability at Site J1007, with the highest opal% for the past 150 kyr found during Termination II and MIS 3 (Figure 5a). At Site J1002, reconstructed opal% shows a prominent peak during Holocene, but remains low and stable before Last Glacial Maximum (LGM, 23-19 ka) (Figure 5b). At Site J1002, opal% only ranges ~1% before the LGM, which can be almost entirely attributed to reconstruction uncertainty (2*RMSD=1.36%, see pink shading in Figure 5). Thus, we caution against the utility of the J1002 opal% reconstruction before the LGM and do not use it for paleoceanographic interpretation.

Over the past 30 kyr, opal% at J1007 and J1002 gradually increases from the last glacial period to the Holocene. During the late Holocene, J1007 opal% is 4-5%, similar to the opal content of ~5% in nearby surface sediments (Romero and Hebbeln, 2003). Meanwhile, J1002 opal% of about 2.5% during the Holocene agrees with opal contents of ~4% in surface sediments at 44°S (Chase et al., 2015; Romero and Hebbeln, 2003). The opal% range for J1007 over the last 30 kyr (2-6%) is similar to that of two nearby sites, and the variation trend mimics GeoB 3395-3. At Site J1002, the low opal% prior to the last glacial period is attributable to a marked increase in sedimentation rate (>3 m/kyr), which appears to significantly dilute the opal% relative to the Holocene.

Previous opal% reconstructions along the Chilean Margin only covered the past 30 kyr, and most vary in a similar range but with different patterns. On the central Chilean Margin, site GeoB 3395-3 (35°13′S, 72°48.5′W, 678 m) has opal% ranging from ~1.5-5% for the past 23 kyr, with the highest values appearing during late Holocene (Romero and Hebbeln, 2003; Romero et al., 2006). The opal% at ODP Site 1234 (36°14′S, 73°41′W, 1015 m) range from ~2-5% for the last 30 kyr, with peak values occurring during the last glacial period (26-20 ka), but slightly before LGM (Chase et al., 2014). Moreover, it is worth noting that the chlorins content at nearby site GeoB 7165-1 (36°33′S, 73° 40′W, 797 m) also increases from the LGM to late Holocene (Mohtadi et al., 2008). Further south, the diatom abundance record from ODP Site 1233 (41°S, 74°27′W, 838 m) is very similar to that of ODP 1234 (Chase et al., 2014). Overall, the consistent range of reconstructed opal% at J1002 and J1007 with nearby sites strongly support the robustness of spectral G/B-opal% proxy.

3.3 Sedimentary U/Th

In nature, thorium occurs almost entirely as ^{232}Th while uranium primarily exists as ^{238}U, both of which are primarily supplied to the oceans by riverine runoff (McManus et al., 2006). As a non-redox-sensitive metal, ^{232}Th has low solubility in rivers and oceans, and is largely absorbed on the surface of clay minerals (Harmsen et a., 1980). On the other hand, ^{238}U exist as both soluble U(VI) and insoluble U(IV) phases (Langmuir, 1978). In oxygenated seawater, ^{238}U is present dominantly as a stable U(VI) carbonate complex, with a small fraction associated with particulate organic carbon flux (McManus et al., 2005). Under suboxic conditions, authigenic U accumulates in the sediments as a combination of the bio-authigenic phase associated with settling organic particles and that formed by diffusion of U into sedimentary pore waters (Barnes and Cochran, 1990; Henderson and Anderson, 1999; McManus et al., 2005). Therefore, sedimentary U/Th, which minimizes the influence of variable detrital sources and sedimentation rates (thus the authigenic U burial rate), can be used as a non-quantitative indicator of redox conditions of the sediments.

Both the thorium and uranium contents are higher at Site J1002 than Site J1007, corresponding to larger terrestrial input to the south Chilean Margin. In contrast, U/Th at Site J1007 was found to be higher than that of J1002 (Figure 5). Higher U/Th reflects more suboxic sedimentary conditions (referring to low dissolved oxygen availability in bottom waters), high organic carbon rain rates, or some combination of both processes (McManus et al., 2006). We observe marked similarities in both trends and magnitudes between measured opal%, G/B-reconstructed opal%, and U/Th profiles at both sites (Figure 5). The co-occurrence of high productivity intervals (high opal %, high G/B) and suboxic conditions, as indicated by high U/Th, supports the use of G/B as a proxy of diatom productivity on the Chilean Margin.

3.4 Reconstructed opal MAR

Previous studies along the Chilean Margin provide only short and relatively low-resolution records of opal MAR (Chase et al., 2014; Hebbeln et al., 2002; Mohtadi et al., 2004; Romero et al., 2006). To fill the research gap on sub-orbital-scale variability in diatom productivity, we generated opal MAR records with G/B-derived opal% from Site J1007. Opal MAR was calculated as:

$$\text{Opal MAR} = \text{opal\%} * \rho_{dry} * \text{LSR} \qquad \text{(Eq. 1)}$$

where the opal% is calculated from the calibrated spectral G/B ratio, ρ_{dry} is the shipboard-measured dry bulk density of the sediment (g/cm^3), and LSR is the linear sedimentation rate (cm/kyr) as established by J1007 age model.

In general, the sedimentary record of opal MAR shows large-amplitude variation at Site J1007 (Figure 6). Over the last 30 kyr, opal MAR of 2-3 g/cm^2/kyr were found before the LGM, which decreased to ~1 g/cm^2/kyr during the deglaciation and into the Holocene. The opal flux records from two adjacent sites (GeoB 3395-3 and ODP Site 1234) show a distinct peak of ~1.5 g/cm^2/kyr during the LGM (Figure 6a; Chase et al., 2014; Romero et al., 2006). Further south, opal MAR from ODP Site 1233 reaches a peak during the last glacial period (1.8 g/cm^2/kyr) and decreases below 0.2 g/cm^2/kyr since 20 ka (Chase et al., 2014). Note that ^{230}Th normalization was applied to opal MAR calculations at ODP Site 1234 and ODP Site 1233, but not at GeoB 3395-3. The opal MAR variation of Site J1007 shows higher levels with longer duration than observed at the other three nearby sites. The difference may be due to the difference in the data sources. The J1007 record is based on continuous high-resolution G/B ratio, whereas the other records are based on low-resolution discrete wet analyses (Figure 5). In fact, comparing the latter with our discrete samples from J1007 suggests a greater consistency among the record in terms of regional changes in opal productivity. We note, however, that changes in sedimentation rate at Site J1007 impart the largest influence on the opal MAR, and the broad peak reflects this.

On a longer timescale, the most outstanding features of the Site J1007 opal MAR record are two large peaks, one at ~50 ka and a secondary peak that we tentatively place at Termination II based on benthic δ^{18}O tuning (Figure 3; Figure 6b). Similar opal flux maxima during MIS 3 have been documented at the site of V19-30 (Figure 6b) and other sites in the EEP (e.g., TR163-31, ME-24) (Dubois et al., 2010; Kienast et al., 2007; Hayes et al., 2011). These opal MAR changes along the eastern Pacific basin are further echoed by a Diol index record offshore Southeastern Australia, which infers maximum *Proboscia* diatom abundance during MIS stages 1, 3 and 5e (Lopes dos Santos et al., 2012).

Enhanced opal preservation related to EEP dust flux (Dubois et al., 2010) and increased contribution of northern hemisphere waters with higher Si:N (Hayes et al., 2011; Kienast et al., 2007) have been discussed as possible drivers for the 50 ka flux peak in the EEP. However, our new opal MAR record from the mid-latitudes clearly refute both the EEP dust controlled or Northern Hemisphere-sourced mechanisms. This common 50 ka event along the eastern Pacific meridional transect, paired with a peak diatom productivity offshore Southeastern Australia, implies a climatic connection between the high and low latitudes in the Southern Hemisphere, likely through nutrient-rich intermediate waters exported from the Pacific-sector of the Southern Ocean (Talley, 2013). Southern Ocean Intermediate Waters supply nitrogen, phosphorous, and silicate to the global thermocline, thereby supporting up to 75% of tropical production (Ayers et al., 2013; Sarmiento et al., 2004). The widely presented MIS 3 opal flux peak supports the idea of enhanced Si supply to low latitudes (Hayes et al., 2011), depicting a clear route of "oceanic tunneling" between the Antarctic and the equatorial Pacific (Pena et al., 2008; Spero and Lea, 2002). Moreover, the opal flux at Site J1007 is nearly ten times greater that of EEP records, implying that mid-latitude continental margins could have served as an important sink for leaking Si from the glacial Southern Ocean (Bradtmiller et al., 2009).

4. Conclusions

Diatom production plays a major role in the biological pump, especially in the Southern Ocean and upwelling regions such as along the EEP and western margins of South American. However, because measuring opal% in sediment is analytically very laborious, obtaining high resolution sedimentary records of opal accumulation is practically impossible, especially in cores with very high-sedimentation rates like those along the Chilean Margin. This study demonstrates that using shipboard measurements of the spectral G/B ratio from newly recovered sediment cores on the Chilean Margin, coupled with calibration of discrete samples using traditional methods, can offer a new approach to generate high-resolution paleoceanographic records for reconstructing glacial-interglacial changes in South Pacific diatom productivity. In more detail, we conclude the following:

1. The spectral green/blue (G/B) ratio in Chilean Margin sediments can serve as an efficient shipboard stratigraphic tool, where other shipboard data (e.g., magnetic susceptibility) are not conclusive.
2. The G/B records provide high-resolution proxy records for regional changes in diatom productivity over time. The conversion of G/B data to opal% records requires site-specific calibrations from discrete opal% analysis using traditional wet-alkaline digestive methods. Offsets among sites in the G/B ratio to opal% relationships are likely related to lithological effects. Nevertheless, the records suggest that, despite diagenetic effects on biogenic silica and organic matter preservation, the G/B records may more reliably record paleoproductivity, especially in very high sedimentation rates environments where their concentration are diluted.
3. Continuous records of opal mass accumulation rate on the Chilean Margin over the last ~150,000 years largely tracks existing records from the EEP, with a common opal flux peak at ~50 ka. This suggests a climatic link between high and low latitudes in the South Pacific through intermediate waters.

Core Name	Latitude	Longitude	Water Depth (m)	Reference
J1002	46° 4.30′	75° 41.23′W	1534	This study
J1007	36° 32.54′	73° 39.99′W	808	This study
ODP Site 1233	41°S	74°27′W	838	Chase et al, 2014
ODP Site 1234	36°14′S	73°41′W	1051	Chase et al, 2014
GeoB 3395-3	35°13′S	72°48.5′W	678	Romero et al., 2006
V19-30	3°22.98′	83°31.02′W	3091	Hayes et al., 2011

Table 1. Site locations in Figure 1

FIGURES AND CAPTIONS

Figure 1. Map of the South Pacific and study region. A. Core locations of J1002, J1007, and other sites discussed in this paper (Table 1). Black arrows show the path of the Southern Ocean Intermediate Water, the surface flow of the Antarctic Circumpolar Current, and the Peru-Chile Current. B. Zoomed-in view of the Chilean Margin (red box in A), with core locations superimposed on mean annual sea-surface chlorophyll-a concentration. J1002 (red), ODP Site 1233 (light blue), J1007 (green), ODP Site 1234 (orange), and GeoB 3395-3 (light purple) are shown. Chlorophyll-a data are from the MODIS-Aqua Level 3 database.

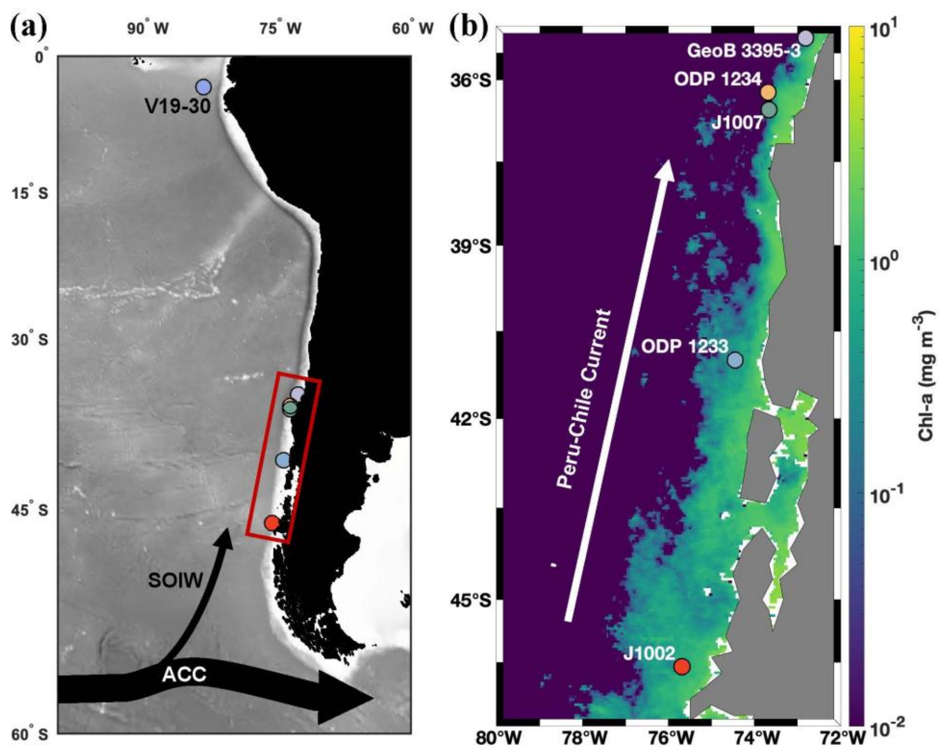

Figure 2. Core photos and smear slide photos representing intervals with high and low G/B values Site J1002 (A) and Site J1007 (B). Core photos were taken by line-scan camera on SHIL and smear slide photos under microscope during Expedition 379T. Greener sedimentary intervals (top core sections in both panels) and bluer sedimentary intervals (bottom core sections in both panels) for each site are evident from visual inspection. In both A and B, smear slide photos in the left panels show intervals with abundant diatom presence, corresponding to greener sedimentary intervals, whereas the right panel smear slide images reflect low diatom abundance intervals from bluer intervals. Black arrows show typical diatoms observed in smear slides.

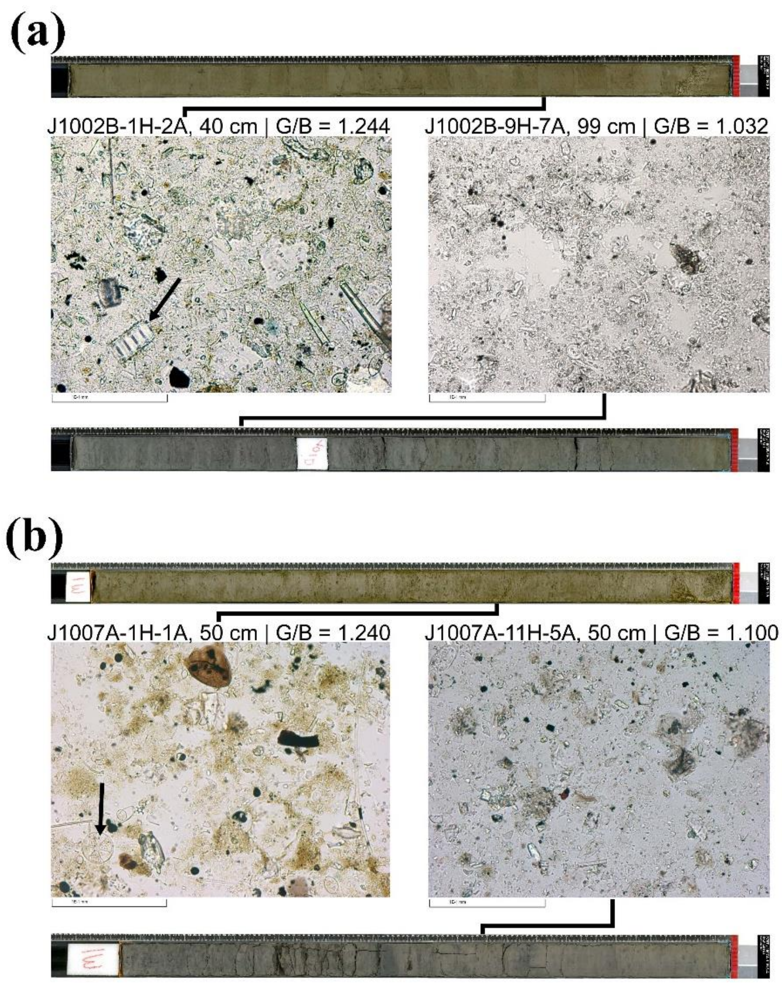

Figure 3. Stratigraphic correlations between Antarctic ice core $\delta^{18}O$ (EDML, EPICA Community Members, 2006), LR04 benthic stack (Lisiecki and Raymo, 2005), the G/B, and benthic $\delta^{18}O$ for Site J1007 (A) and Site J1002 (B). Age control points from ^{14}C ages are displayed (yellow diamonds). Tie points for visual correlation between benthic $\delta^{18}O$ and LR04 are denoted by vertical dashed lines.

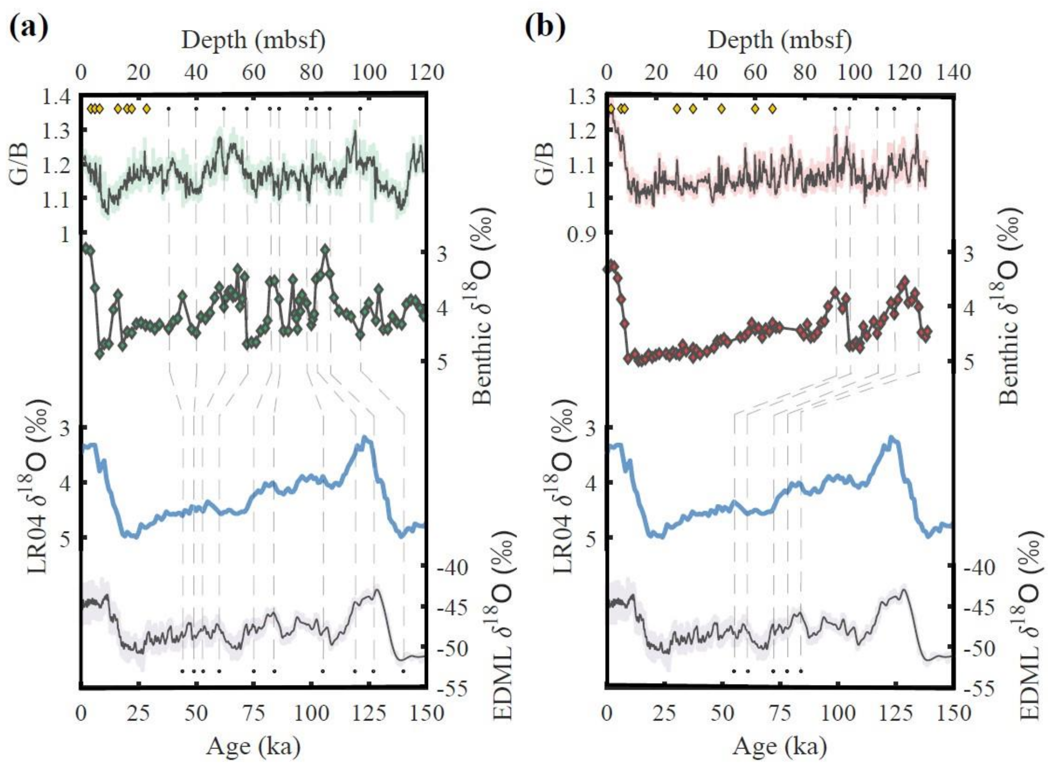

Figure 4. Calibration of the G/B proxy. A. Correlation between opal% and the spectral G/B ratio for Site J1002 (red squares) and Site J1007 (green circles). B. Correlation between opal% and C_{org}% for Site J1007. C. Correlation between C_{org}% and spectral G/B ratio for Site J1007. Open symbols in all panels represent potentially underestimated opal% data points from low magnetic susceptibility intervals. Shaded areas represent the 95% confidence interval for each regression.

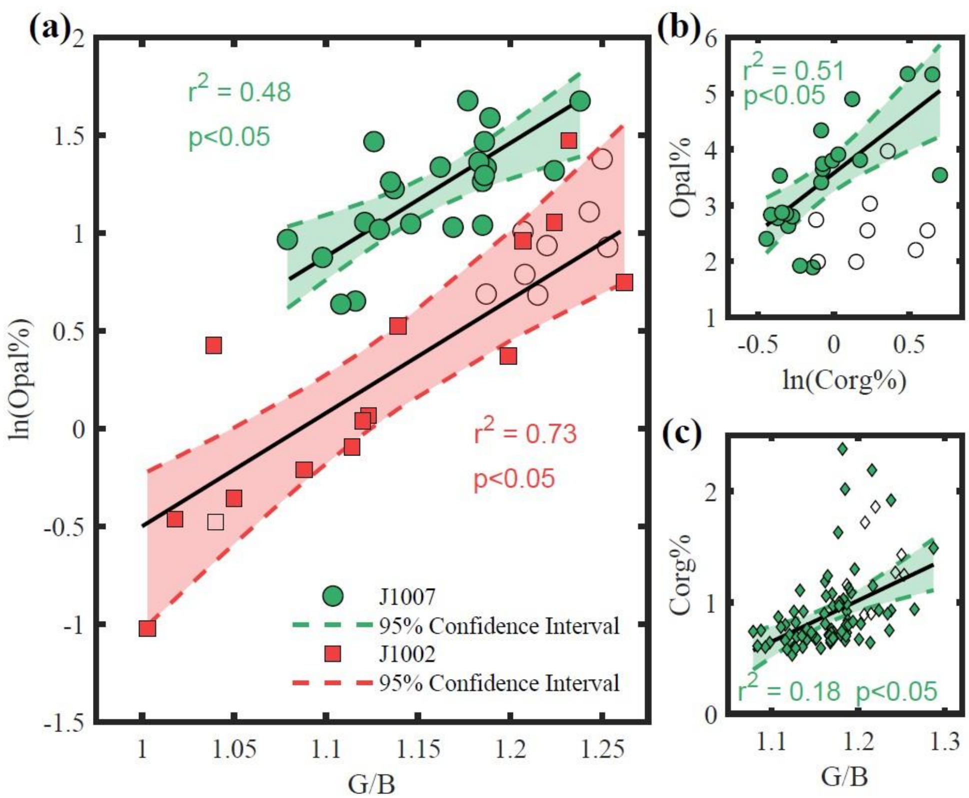

Figure 5. Downcore opal%, U/Th, and magnetic susceptibility records for Site J1007 (A) and Site J1002 (B). Reconstructed opal% for the last ~150 ka at J1007 (green) and 90 ka at J1002 (red) are shown as smoothed solid curves (MATLAB loess smoothing, window = 50) with the ±1 RMSD envelope. Measured opal% (green circles for J1007, red squares for J1002) are superimposed on each reconstructed record. Grey symbols represented potentially underestimated opal% data points from low magnetic susceptibility intervals. The standard error of opal% measurements (0.35%, based on 14 duplicate measurements) was shown as error bar on each data point. Note that we reject those from the calibrations but this does not affect our interpretations of the G/B records. U/Th records are presented as solid grey lines. Magnetic susceptibility at Site J1007 (blue) and Site J1002 (orange) are shown as smoothed solid curves (MATLAB loess smoothing, window = 50). Vertical grey bars denote intervals of low MS coinciding with underestimated opal% data at each site.

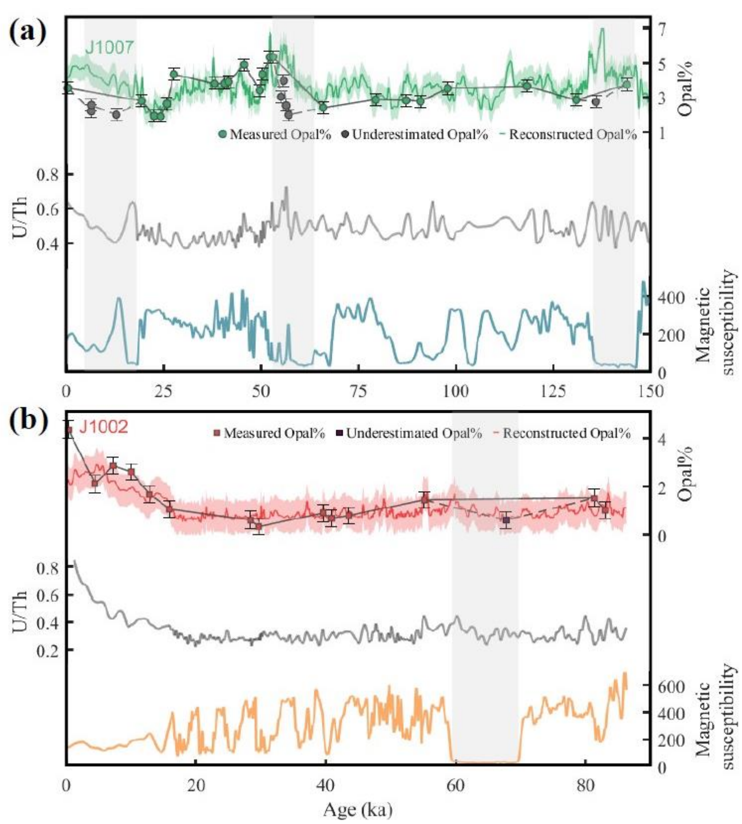

Figure 6. Downcore opal MAR records from the eastern Pacific Ocean. A. Opal MAR variation for the last 30 ka at GeoB3395-3 (yellow; Romero et al., 2006), ODP Site 1234 (pink; Chase et al., 2014), and ODP Site 1233 (blue; Chase et al., 2014). Site J1007 (green) opal MAR are shown as smoothed solid curves (MATLAB loess smoothing, window = 50) with the ±1 uncertainty envelope (by error propagation from 1 RMSD). Grey markers show opal MAR calculated from measured opal% (closed circle) and data points from low magnetic susceptibility (open circle). B. Opal MAR variation for the last 150 ka at Site J1007 (green) and V19-30 (orange; Hayes et al., 2011). Linear sedimentation rate (LSR) for Site J1007 is shown in the bottom panel. The MIS 3 peak in opal flux is highlighted with pink shadings. The dashed arrow shows potential correlation between the Site J1007 and EEP opal MAR peak at Termination II based on benthic $\delta^{18}O$ tuning.

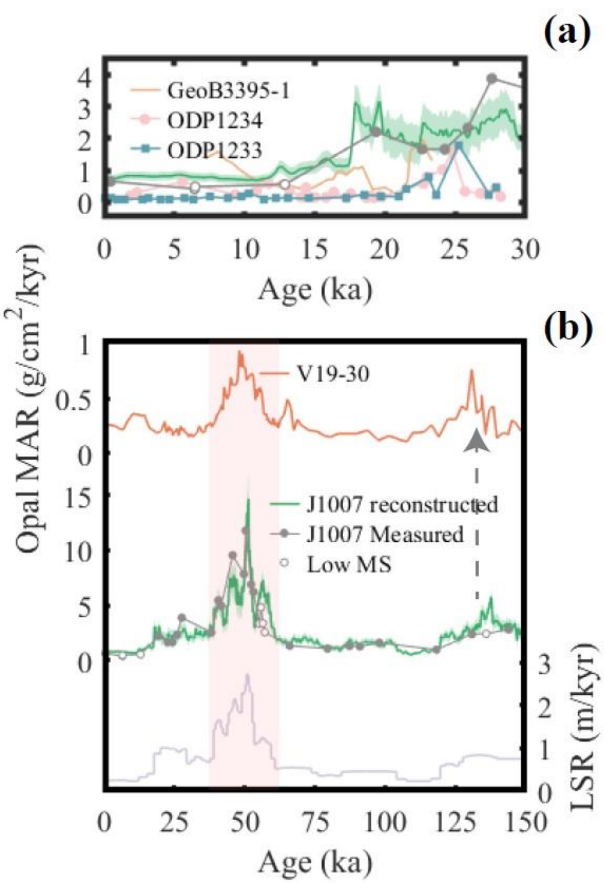

Acknowledgments

We would like to thank the captain and crew of the D/V *JOIDES Resolution* and JRSO for their tireless efforts during the inaugural JR100 expedition. C.L., V.J.C., and Y.R. designed the experiment. C.L. and V.J.C. carried out shore-based geochemical analyses, prepared figures, and wrote the manuscript. S.C.B., Y.R., and L.B.C. organized and managed the expedition. J.D.W. co-led shipboard stratigraphic efforts with G/B. Expedition 379T Scientists assisted in the collection of G/B data and interpretation of shipboard sedimentological data. All authors contributed to the interpretation of shipboard data. The expedition was funded by NSF grant OCE-1756241. This study was funded by NSF grant OCE-1756241 to S.C.B. and Y.R. C.L. was supported by the Chinese Scholarship Council. V.J.C. was supported by the NETL Methane Hydrates Fellowship Program.

Open Research

All data used for this study are available in the supporting information (for peer review), open access database, and cited references.

[†]**Expedition 379T Scientists (those not listed above):** Ivano W. Aiello[1], Alejandro Avila[2], William Biggs[3], Christopher D. Charles[4], Anson H. Cheung[5], Kimberly deLong[6], Isabel A. Dove[7], Xiaojing Du[5,8], Emily R. Estes[9], Ursula Fuentes[10], Cristina García-Lasanta[11], Steven L. Goldstein[12], Anna Golub[13], Julia Rieke Hagemann[14], Robert G. Hatfield[15], Laura L. Haynes[16], Anya V. Hess[17], Nil Irvali[18], Yael Kiro[19], Minda M. Monteagudo[20], Jonathan E. Lambert[12], William M. Longo[21,22], Sarah McGrath[5], Hailey Riechelson[3], Rebecca S. Robinson[7], John Sarao[23], Adam D. Sproson[24], Shawn Taylor[25], Yusuke Yokoyama[26], and Siyao M. Yu[17].

[1]Moss Landing Marine Laboratories, Moss Landing, California, USA. [2]Center for Oceanographic Research in the Eastern South Pacific (FONDAP-COPAS), University of Concepción, Concepción, Chile. [3]Department of Marine and Coastal Sciences, Rutgers University, New Brunswick, New Jersey, USA. [4]Scripps Institution of Oceanography, University of California, San Diego, La Jolla, California, USA. [5]Department of Earth, Environmental, and Planetary Sciences, Brown University, Providence, Rhode Island, USA. [6]Ocean Sciences Department, University of California, Santa Cruz, Santa Cruz, California, USA. [7]University of Rhode Island Graduate School of Oceanography, Narragansett, Rhode Island, USA. [8]Institute at Brown for Environment and Society, Providence, Rhode Island, USA. [9]International Ocean Discovery Program, Texas A&M

University, College Station, Texas, USA. [10]Hydrographic and Oceanographic Services, Chilean Navy, Valparaíso, Chile. [11]Geology Department, Western Washington University, Bellingham, Washington, USA. [12]Lamont-Doherty Earth Observatory, Columbia University, Palisades, New York, USA. [13]Department of Geology and Environmental Geoscience, Lafayette College, Easton, Pennsylvania, USA. [14]Department of Marine Geology and Paleontology, Alfred Wegener Institute Helmholtz Center for Polar and Marine Research, Bremerhaven, Germany. [15]Department of Geological Sciences, University of Florida, Gainesville, Florida, USA. [16]Department of Earth Science and Geography, Vassar College, Poughkeepsie, New York, USA. [17]Department of Earth and Planetary Sciences, Rutgers University, New Brunswick, New Jersey, USA. [18]Department of Earth Science and Bjerknes Centre for Climate Research, University of Bergen, Bergen, Norway. [19]Department of Earth and Planetary Sciences, Weizmann Institute of Science, Rehovot, Israel. [20]School of Earth and Atmospheric Sciences, Georgia Institute of Technology, Atlanta, Georgia, USA. [21]Department of Environmental Studies, Macalester College, Saint Paul, Minnesota, USA. [22]Division of Environmental Health Sciences, University of Minnesota, Minneapolis, Minnesota, USA. [23]College of Geosciences, Texas A&M University, College Station, Texas, USA. [24]Biogeochemistry Research Center, JAMSTEC, Yokosuka, Japan. [25]Department of Geological Sciences and Environmental Studies, Binghamton University, Binghamton, New York, USA. [26]Atmosphere and Ocean Research Institute, The University of Tokyo, Chiba, Japan.

References

Abrantes, F., Lopes, C., Mix, A., & Pisias, N. (2007). Diatoms in Southeast Pacific surface sediments reflect environmental properties. Quaternary Science Reviews, 26(1-2), 155-169. doi:10.1016/j.quascirev.2006.02.022

Anderson, R. F., Ali, S., Bradtmiller, L. I., Nielsen, S. H., Fleisher, M. Q., Anderson, B. E., & Burckle, L. H. (2009). Wind-driven upwelling in the Southern Ocean and the deglacial rise in atmospheric CO_2. Science, 323(5920), 1443-1448. doi:10.1126/science.1167441

Antoine, D., & Morel, A. (1996). Oceanic primary production: 1. Adaptation of a spectral light-photosynthesis model in view of application to satellite chlorophyll observations. Global Biogeochemical Cycles, 10(1), 43-55. doi:10.1029/95GB02831

Ayers, J. M., & Strutton, P. G. (2013). Nutrient variability in Subantarctic Mode Waters forced by the Southern Annular Mode and ENSO. Geophysical Research Letters, 40(13), 3419-3423. doi:10.1002/grl.50638

Barbante, C., Barnola, J.-M., Becagli, S., Beer, J., Bigler, M., Boutron, C., . . . Chappellaz, J. (2006). One-to-one coupling of glacial climate variability in Greenland and Antarctica. Nature, 444(7116), 195-198.

Barnes, C., & Cochran, J. (1990). Uranium removal in oceanic sediments and the oceanic U balance. Earth and Planetary Science Letters, 97(1-2), 94-101.

Bova, S.C., Rosenthal, Y., Childress, L.B., and Expedition 379T Scientists (2021), Digging Deeper with the JR100: Extending high resolution paleoclimate records from the Chilean Margin to the Eemian. Pers. commun., https://zenodo.org/record/5553428#.YV4q6y2cbIE

Bradtmiller, L. I., Anderson, R. F., Fleisher, M. Q., & Burckle, L. H. (2009). Comparing glacial and Holocene opal fluxes in the Pacific sector of the Southern Ocean. Paleoceanography, 24(2), n/a-n/a. doi:10.1029/2008pa001693

Brzezinski, M. A. (2002). A switch from $Si(OH)_4$to NO_3^-depletion in the glacial Southern Ocean. Geophysical Research Letters, 29(12). doi:10.1029/2001gl014349

Charles, C. D., Froelich, P. N., Zibello, M. A., Mortlock, R. A., & Morley, J. J. (1991). Biogenic opal in Southern Ocean sediments over the last 450,000 years: Implications for surface water chemistry and circulation. Paleoceanography, 6(6), 697-728. doi:10.1029/91PA02477

Chase, Z., Kohfeld, K. E., & Matsumoto, K. (2015). Controls on biogenic silica burial in the Southern Ocean. Global Biogeochemical Cycles, 29(10), 1599-1616. doi:10.1002/2015gb005186

Chase, Z., McManus, J., Mix, A. C., & Muratli, J. (2014). Southern-ocean and glaciogenic nutrients control diatom export production on the Chile margin. Quaternary Science Reviews, 99, 135-145. doi:10.1016/j.quascirev.2014.06.015

Clementi, V. J., & Sikes, E. L. (2019). Southwest Pacific Vertical Structure Influences on Oceanic Carbon Storage Since the Last Glacial Maximum. Paleoceanography and Paleoclimatology, 34(5), 734-754. doi:10.1029/2018PA003501

Conley, D. J., & Schelske, C. L. (2001). Biogenic Silica. In J. P. Smol, H. J. B. Birks, W. M. Last, R. S. Bradley, & K. Alverson (Eds.), Tracking Environmental Change Using Lake Sediments: Terrestrial, Algal, and Siliceous Indicators (pp. 281-293). Dordrecht: Springer Netherlands.

de Bar, M. W., Stolwijk, D. J., McManus, J. F., Sinninghe Damsté, J. S., & Schouten, S. (2018). A Late Quaternary climate record based on long-chain diol proxies from the Chilean margin. Climate of the Past, 14(11), 1783-1803. doi:10.5194/cp-14-1783-2018

De Vleeschouwer, D., Dunlea, A. G., Auer, G., Anderson, C. H., Brumsack, H., de Loach, A., . . . Jang, K. (2017). Quantifying K, U, and T h contents of marine sediments using shipboard natural gamma radiation spectra measured on DV JOIDES R esolution. Geochemistry, Geophysics, Geosystems, 18(3), 1053-1064.

DeMaster, D. J., 1979. The marine budgets of silica and Ph.D. Dissertation, Yale University, 308 pp.

Dubois, N., Kienast, M., Kienast, S., Calvert, S. E., François, R., & Anderson, R. F. (2010). Sedimentary opal records in the eastern equatorial Pacific: It is not all about leakage. Global Biogeochemical Cycles, 24(4), n/a-n/a. doi:10.1029/2010gb003821

Hayes, C. T., Anderson, R. F., & Fleisher, M. Q. (2011). Opal accumulation rates in the equatorial Pacific and mechanisms of deglaciation. Paleoceanography, 26(1). doi:10.1029/2010pa002008

Hebbeln, D., Lamy, F., Mohtadi, M., & Echtler, H. (2007). Tracing the impact of glacial-interglacial climate variability on erosion of the southern Andes. Geology, 35(2). doi:10.1130/g23243a.1

Hebbeln, D., Marchant, M., & Wefer, G. (2002). Paleoproductivity in the southern Peru-Chile Current through the last 33 000 yr. Marine Geology, 186(3-4), 487-504. doi:Pii S0025-3227(02)00331-6

Hebbeln, D., Marchant, M., Freudenthal, T., & Wefer, G. (2000). Surface sediment distribution along the Chilean continental slope related to upwelling and productivity. Marine Geology, 164(3-4), 119-137. doi:10.1016/s0025-3227(99)00129-2

Henderson, G. M., & Anderson, R. F. (2003). The U-series toolbox for paleoceanography. Reviews in mineralogy and geochemistry, 52(1), 493-531.

Heusser, L., Heusser, C., Mix, A., & McManus, J. (2006). Chilean and Southeast Pacific paleoclimate variations during the last glacial cycle: directly correlated pollen and δ18O records from ODP Site 1234. Quaternary Science Reviews, 25(23-24), 3404-3415. doi:10.1016/j.quascirev.2006.03.011

Jouzel, J., Masson-Delmotte, V., Cattani, O., Dreyfus, G., Falourd, S., Hoffmann, G., . . . Wolff, E. W. (2007). Orbital and Millennial Antarctic Climate Variability over the Past 800,000 Years. Science, 317(5839), 793. doi:10.1126/science.1141038

Kaiser, J., Lamy, F., Arz, H. W., & Hebbeln, D. (2007). Dynamics of the millennial-scale sea surface temperature and Patagonian Ice Sheet fluctuations in southern Chile during the last 70kyr (ODP Site 1233). Quaternary International, 161(1), 77-89. doi:10.1016/j.quaint.2006.10.024

Kienast, S. S., Kienast, M., Mix, A. C., Calvert, S. E., & François, R. (2007). Thorium-230 normalized particle flux and sediment focusing in the Panama Basin region during the last 30,000 years. Paleoceanography, 22(2). doi:10.1029/2006pa001357

Kuczynska, P., Jemiola-Rzeminska, M., & Strzalka, K. (2015). Photosynthetic Pigments in Diatoms. Marine Drugs, 13(9). doi:10.3390/md13095847

Lamy, F., Hebbeln, D., & Wefer, G. (1998). Terrigenous sediment supply along the Chilean continental margin: modern regional patterns of texture and composition. Geologische Rundschau, 87(3), 477-494. doi:10.1007/s005310050223

Lamy, F., Kaiser, J., Ninnemann, U., Hebbeln, D., Arz, H. W., & Stoner, J. (2004). Antarctic timing of surface water changes off Chile and Patagonian ice sheet response. Science, 304(5679), 1959-1962. doi:10.1126/science.1097863

Lisiecki, L. E., & Raymo, M. E. (2005). A Pliocene-Pleistocene stack of 57 globally distributed benthic δ18O records. Paleoceanography, 20(1), n/a-n/a. doi:10.1029/2004pa001071

Lopes dos Santos, R. A., Wilkins, D., De Deckker, P., & Schouten, S. (2012). Late Quaternary productivity changes from offshore Southeastern Australia: A biomarker approach. Palaeogeography, Palaeoclimatology, Palaeoecology, 363-364, 48-56. doi:10.1016/j.palaeo.2012.08.013

López-Otálvaro, G.-E., Flores, J.-A., Sierro, F. J., & Cacho, I. (2008). Variations in coccolithophorid production in the Eastern Equatorial Pacific at ODP Site 1240 over the last seven glacial–interglacial cycles. Marine Micropaleontology, 69(1), 52-69. doi:10.1016/j.marmicro.2007.11.009

Lougheed, B. C., & Obrochta, S. P. (2019). A Rapid, Deterministic Age-Depth Modeling Routine for Geological Sequences With Inherent Depth Uncertainty. Paleoceanography and Paleoclimatology, 34(1), 122-133. doi:10.1029/2018pa003457

Matsumoto, K., Sarmiento, J. L., & Brzezinski, M. A. (2002). Silicic acid leakage from the Southern Ocean: A possible explanation for glacial atmosphericpCO2. Global Biogeochemical Cycles, 16(3), 5-1-5-23. doi:10.1029/2001gb001442

McManus, J., Berelson, W. M., Klinkhammer, G. P., Hammond, D. E., & Holm, C. (2005). Authigenic uranium: Relationship to oxygen penetration depth and organic carbon rain. Geochimica et Cosmochimica Acta, 69(1), 95-108. doi:10.1016/j.gca.2004.06.023

McManus, J., Berelson, W. M., Severmann, S., Poulson, R. L., Hammond, D. E., Klinkhammer, G. P., & Holm, C. (2006). Molybdenum and uranium geochemistry in continental margin sediments: Paleoproxy potential. Geochimica et Cosmochimica Acta, 70(18), 4643-4662. doi:10.1016/j.gca.2006.06.1564

Mix, A. C., Rugh, W., Pisias, N. G., & Veirs, S. (1992). Color reflectance spectroscopy: A tool for rapid characterization of deep-sea sediments. Paper presented at the Proceedings of the Ocean Drilling Program, Part A, Initial report.

Mohtadi, M., & Hebbeln, D. (2004). Mechanisms and variations of the paleoproductivity off northern Chile (24°S-33°S) during the last 40,000 years. Paleoceanography, 19(2), n/a-n/a. doi:10.1029/2004pa001003

Mohtadi, M., Rossel, P., Lange, C. B., Pantoja, S., Böning, P., Repeta, D. J., . . . Brumsack, H.-J. (2008). Deglacial pattern of circulation and marine productivity in the upwelling region off central-south Chile. Earth and Planetary Science Letters, 272(1-2), 221-230. doi:10.1016/j.epsl.2008.04.043

Mortlock, R. A., & Froelich, P. N. (1989). A simple method for the rapid determination of biogenic opal in pelagic marine sediments. Deep Sea Research Part A. Oceanographic Research Papers, 36(9), 1415-1426. doi:https://doi.org/10.1016/0198-0149(89)90092-7

Nederbragt, A. J., Thurow, J. W., & Merrill, R. B. (2000). Color records from the California margin: Proxy indicators for sediment composition and climatic change. Proceedings of the Ocean Drilling Program. Scientific results, 167, 319-329.

Penkrot, M. L., Jaeger, J. M., Cowan, E. A., St-Onge, G., & LeVay, L. (2018). Multivariate modeling of glacimarine lithostratigraphy combining scanning XRF, multisensory core properties, and CT imagery: IODP Site U1419. Geosphere, 14(4), 1935-1960.

Peterson, L. C., Haug, G. H., Hughen, K. A., & Röhl, U. (2000). Rapid changes in the hydrologic cycle of the tropical Atlantic during the last glacial. Science, 290(5498), 1947-1951.

Piola, A. R., & Georgi, D. T. (1982). Circumpolar properties of Antarctic intermediate water and Subantarctic Mode Water. Deep Sea Research Part A. Oceanographic Research Papers, 29(6), 687-711. doi:https://doi.org/10.1016/0198-0149(82)90002-4

Reimer, P. J., Austin, W. E. N., Bard, E., Bayliss, A., Blackwell, P. G., Bronk Ramsey, C., . . . Talamo, S. (2020). The IntCal20 Northern Hemisphere Radiocarbon Age Calibration Curve (0–55 cal kBP). Radiocarbon, 62(4), 725-757. doi:10.1017/rdc.2020.41

Reuss, N. S., Anderson, N. J., Fritz, S. C., & Simpson, G. L. (2013). Responses of microbial phototrophs to late-Holocene environmental forcing of lakes in south-west Greenland. Freshwater Biology, 58(4), 690-704. doi:10.1111/fwb.12073

Reuss, N., Conley, D. J., & Bianchi, T. S. (2005). Preservation conditions and the use of sediment pigments as a tool for recent ecological reconstruction in four Northern European estuaries. Marine Chemistry, 95(3), 283-302. doi:https://doi.org/10.1016/j.marchem.2004.10.002

Robinson, R. S., Mix, A., & Martinez, P. (2007). Southern Ocean control on the extent of denitrification in the southeast Pacific over the last 70ka. Quaternary Science Reviews, 26(1-2), 201-212. doi:10.1016/j.quascirev.2006.08.005

Romero, O. E., Kim, J.-H., & Hebbeln, D. (2017). Paleoproductivity evolution off central Chile from the Last Glacial Maximum to the Early Holocene. Quaternary Research, 65(3), 519-525. doi:10.1016/j.yqres.2005.07.003

Romero, O., & Hebbeln, D. (2003). Biogenic silica and diatom thanatocoenosis in surface sediments below the Peru–Chile Current: controlling mechanisms and relationship with productivity of surface waters. Marine Micropaleontology, 48(1), 71-90. doi:https://doi.org/10.1016/S0377-8398(02)00161-5

Sallée, J.-B., Speer, K., Rintoul, S., & Wijffels, S. (2010). Southern Ocean Thermocline Ventilation. Journal of Physical Oceanography, 40(3), 509-529. doi:10.1175/2009JPO4291.1

Sarmiento, J. L., Gruber, N., Brzezinski, M., & Dunne, J. (2004). High-latitude controls of thermocline nutrients and low latitude biological productivity. Nature, 427(6969), 56-60.

Sigman, D. M., & Boyle, E. A. (2000). Glacial/interglacial variations in atmospheric carbon dioxide. Nature, 407(6806), 859-869. doi:Doi 10.1038/35038000

Sloyan, B. M., & Rintoul, S. R. (2001). The Southern Ocean Limb of the Global Deep Overturning Circulation*. Journal of Physical Oceanography, 31(1), 143-173. doi:10.1175/1520-0485(2001)031<0143:Tsolot>2.0.Co;2

Stauber, J. L., & Jeffrey, S. W. (1988). PHOTOSYNTHETIC PIGMENTS IN FIFTY-ONE SPECIES OF MARINE DIATOMS1. Journal of Phycology, 24(2), 158-172. doi:10.1111/j.1529-8817.1988.tb04230.x

Strub, P. T. (1998). Coastal ocean circulation off Western South America. The Global Coastal Ocean. Regional Studies and Syntheses, 273-315. Retrieved from https://ci.nii.ac.jp/naid/20001225871/en/

Stuut, J. B. W., Marchant, M., Kaiser, J., Lamy, F., Mohtadi, M., Romero, O., & Hebbeln, D. (2006). The late quaternary paleoenvironment of Chile as seen from marine archives. Geogr. Helv., 61(2), 135-151. doi:10.5194/gh-61-135-2006

Talley, L. (2013). Closure of the Global Overturning Circulation Through the Indian, Pacific, and Southern Oceans: Schematics and Transports. Oceanography, 26(1), 80-97. doi:10.5670/oceanog.2013.07

Toggweiler, J. R., Russell, J. L., & Carson, S. R. (2006). Midlatitude westerlies, atmospheric CO2, and climate change during the ice ages. Paleoceanography, 21(2), n/a-n/a. doi:10.1029/2005pa001154

Figure1.

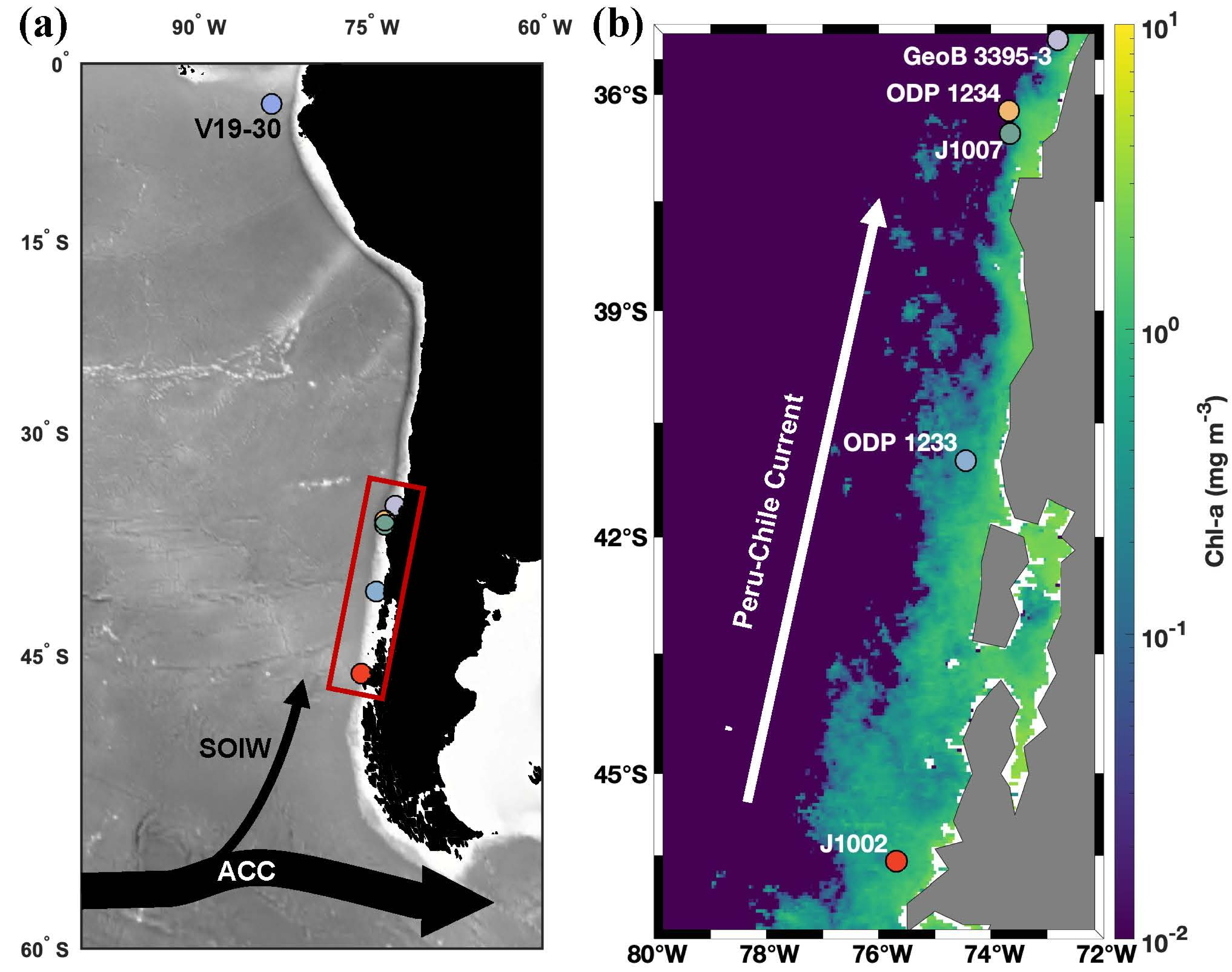
(a)
90° W
75° W
60° W
0°
15° S
30° S
45° S
60° S
V19-30
SOIW
ACC
(b)
GeoB 3395-3
ODP 1234
J1007
ODP 1233
J1002
Peru-Chile Current
36°S
39°S
42°S
45°S
80°W
78°W
76°W
74°W
72°W
10^{1}
10^{0}
10^{-1}
10^{-2}
Chl-a (mg m^{-3})

Figure2.

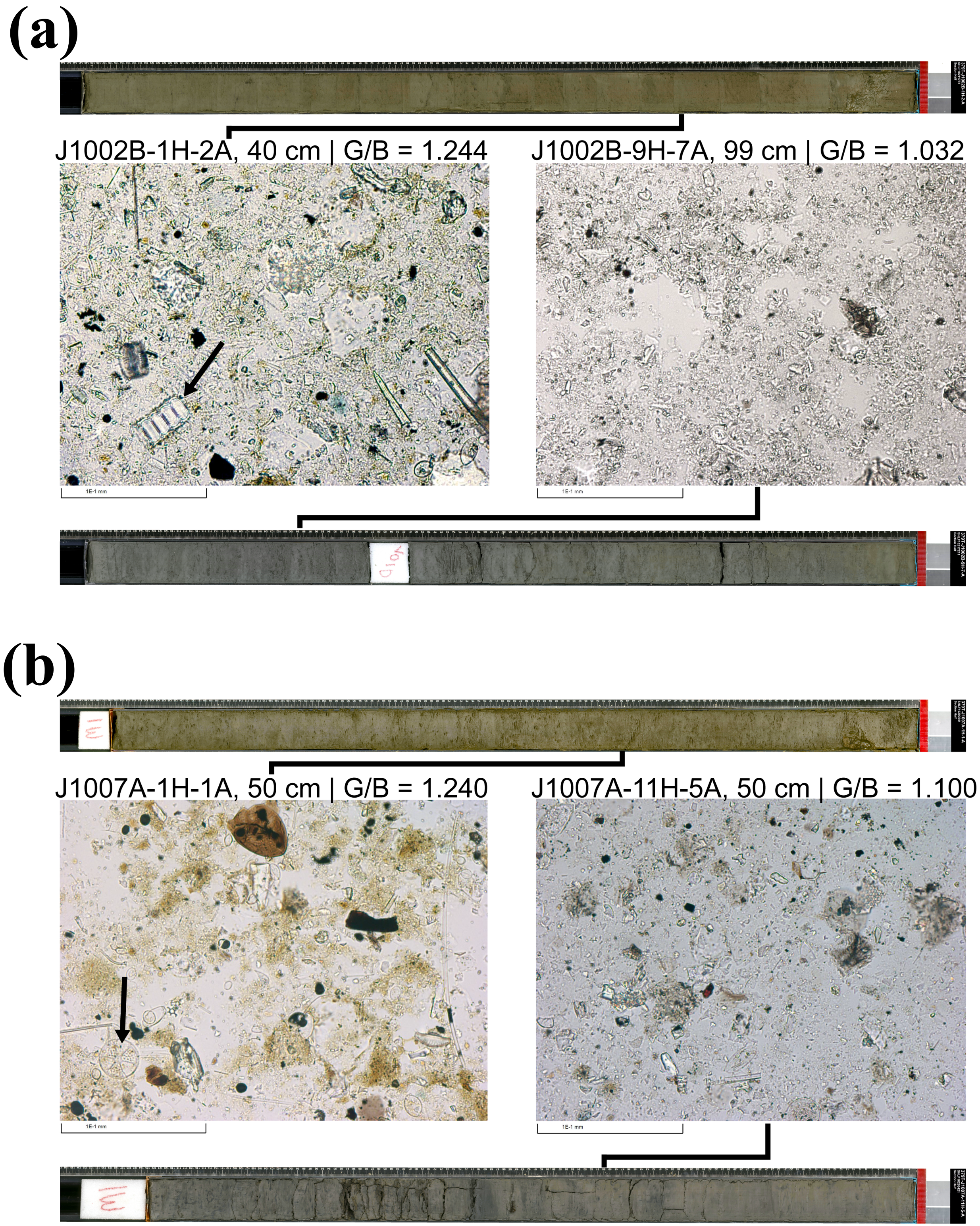
(a)
J1002B-1H-2A, 40 cm | G/B = 1.244
J1002B-9H-7A, 99 cm | G/B = 1.032
1E-1 mm
1E-1 mm
(b)
J1007A-1H-1A, 50 cm | G/B = 1.240
J1007A-11H-5A, 50 cm | G/B = 1.100
1E-1 mm
1E-1 mm

Figure3.

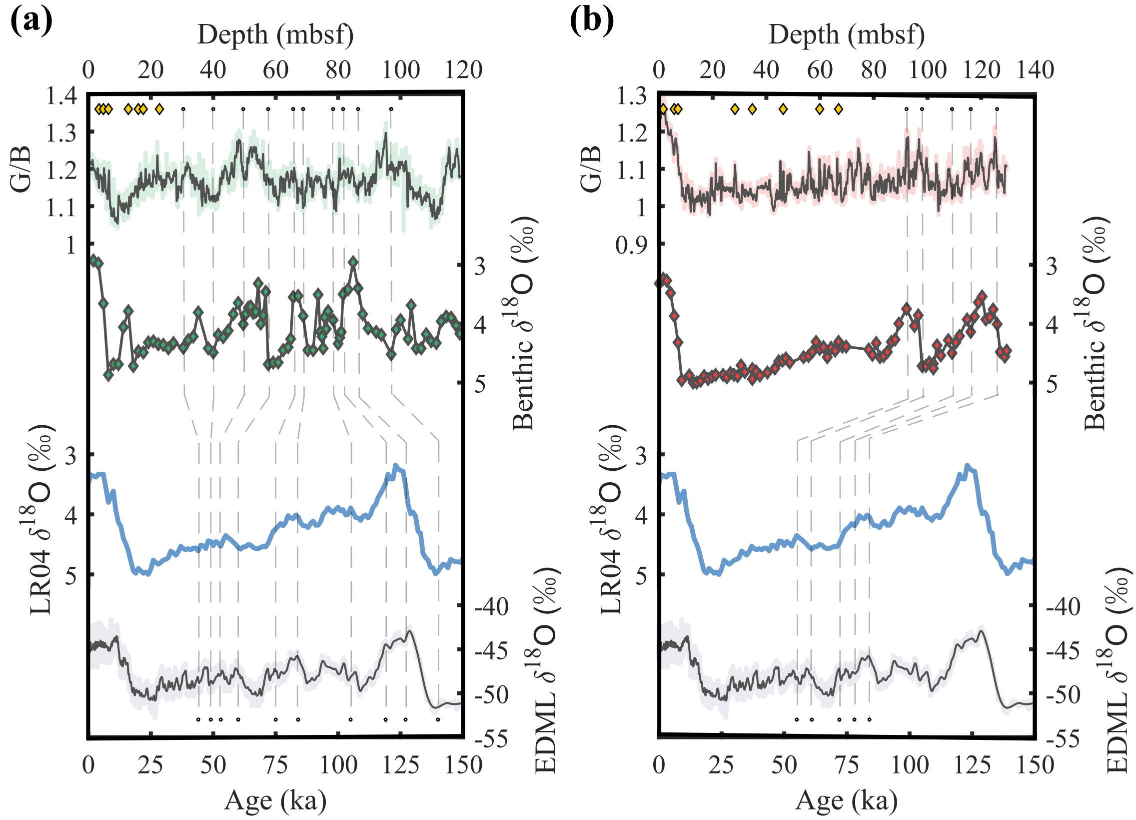

(a)
Depth (mbsf)
G/B
Benthic δ18O (‰)
LR04 δ18O (‰)
EDML δ18O (‰)
Age (ka)
(b)
Depth (mbsf)
G/B
Benthic δ18O (‰)
LR04 δ18O (‰)
EDML δ18O (‰)
Age (ka)

Figure4.

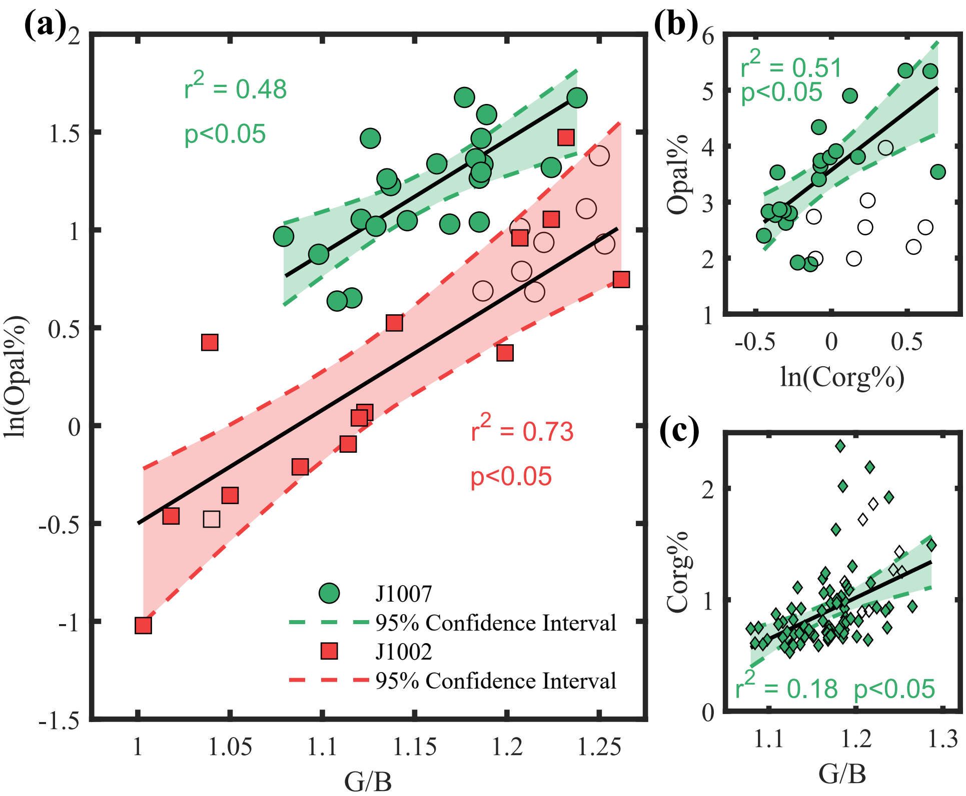

(a)
$r^2 = 0.48$
$p<0.05$
$r^2 = 0.73$
$p<0.05$
J1007
95% Confidence Interval
J1002
95% Confidence Interval
ln(Opal%)
G/B
(b)
$r^2 = 0.51$
$p<0.05$
Opal%
ln(Corg%)
(c)
$r^2 = 0.18$ $p<0.05$
Corg%
G/B

Figure5.

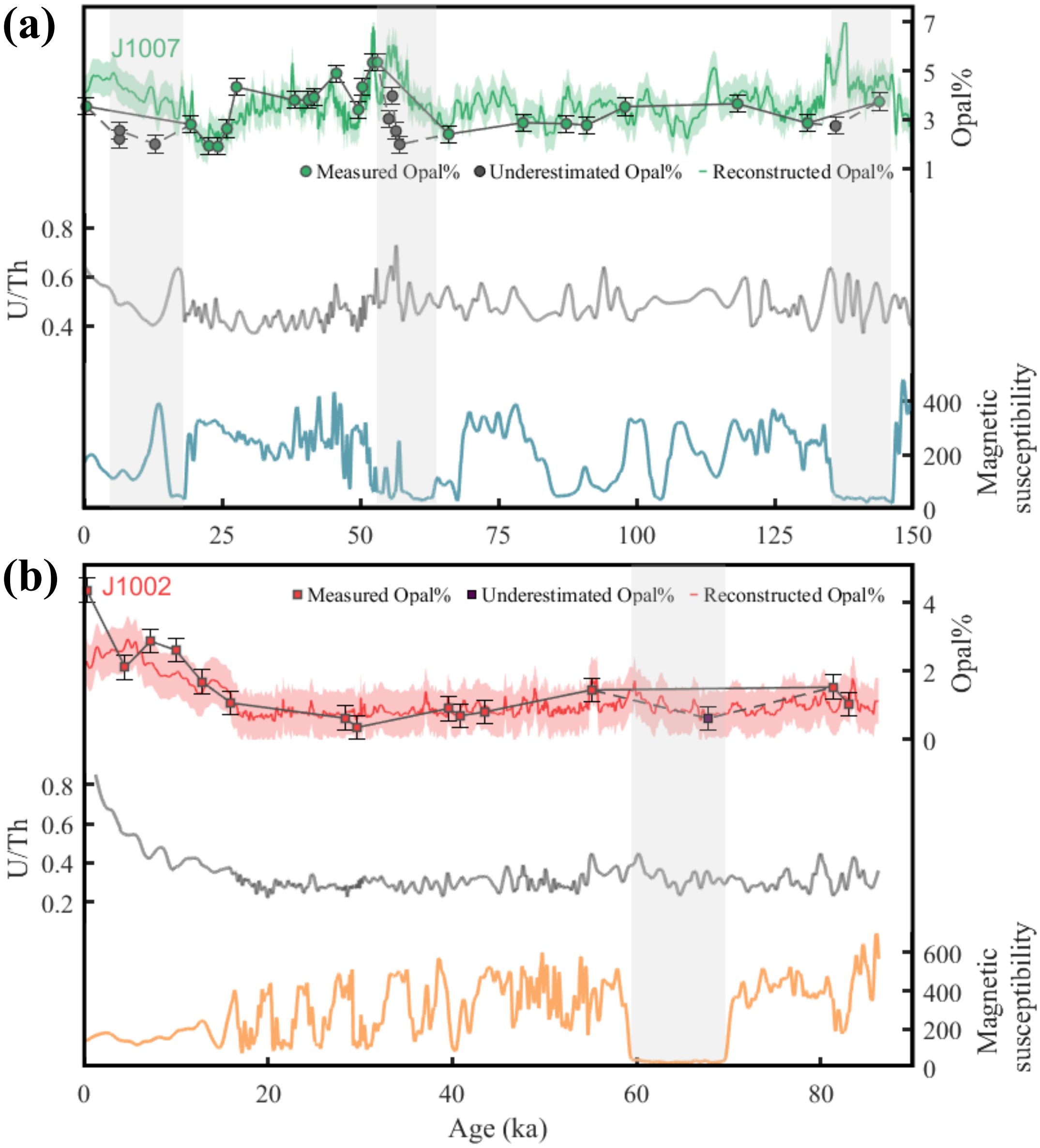

(a)
J1007
Measured Opal%
Underestimated Opal%
Reconstructed Opal%
Opal%
U/Th
Magnetic susceptibility
0
25
50
75
100
125
150
(b)
J1002
Measured Opal%
Underestimated Opal%
Reconstructed Opal%
Opal%
U/Th
Magnetic susceptibility
0
20
40
60
80
Age (ka)

Figure6.

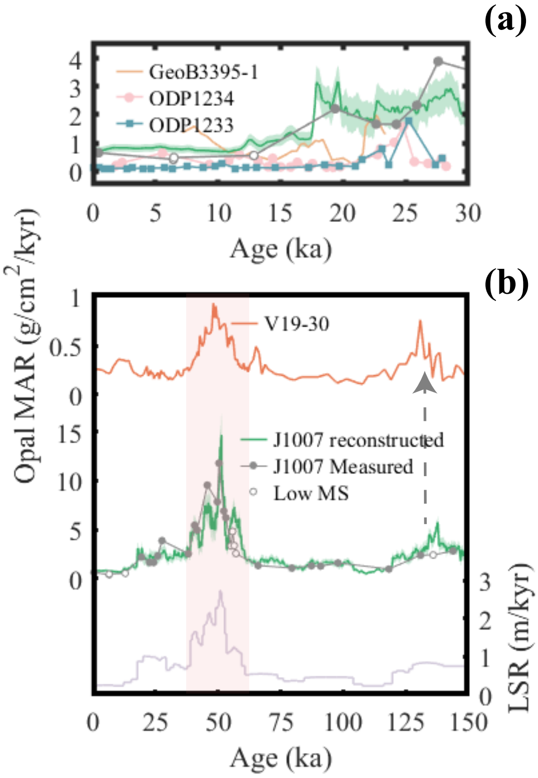

(a)
GeoB3395-1
ODP1234
ODP1233
Age (ka)
Opal MAR (g/cm^2/kyr)
(b)
V19-30
J1007 reconstructed
J1007 Measured
Low MS
LSR (m/kyr)
Age (ka)

[Geochemistry, Geophysics, Geosystems]

Supporting Information for

[The sediment green-blue color ratio as a proxy for biogenic silica productivity along the Chilean Margin.]

[Chen Li[1,2*], Vincent J. Clementi[1*], Samantha C. Bova[1,3], Yair Rosenthal[1,4], Laurel B. Childress[5], James D. Wright[4], Zhimin Jian[2], and Expedition 379T Scientists†]

[[1]Department of Marine and Coastal Sciences, Rutgers University, New Brunswick, New Jersey, USA

[2]State Key Laboratory of Marine Geology, Tongji University, Shanghai, China

[3]Present address: Department of Geological Sciences, San Diego State University, San Diego, California, USA

[4]Department of Earth and Planetary Sciences, Rutgers University, New Brunswick, New Jersey, USA

[5]International Ocean Discovery Program, Texas A&M University, College Station, Texas, USA

†A list of authors and affiliations appears at the end of the paper]

Contents of this file

Additional Supporting Information (Files uploaded separately)

Captions for data set S1 to S2 (upload as separate files)

Introduction

Cores J1002 and J1007 were recovered from the Chilean Margin during the JR100 cruise (D/V JOIDES Resolution Expedition 379T) in 2019. All the experiments conducted in this study were performed at Department of Marine and Coastal Sciences, Rutgers University. This supporting information includes detailed description of biogenic silica measurement, data processing procedure and control points for J1002 and J1007 age models.

Text S1.

Biogenic Silica Measurement

In general, sediment samples were prepared with typical wet-alkaline digestion including "mineral correction" steps modified after Conley et al. (2001). Afterward, dissolved silica was measured by the molybdate blue spectrophotometric method using a modified procedure adapted from Mortlock et al. (1989).

A total of 22 and 41 samples were analyzed for J1002 and J1007, respectively. An addition of three J1001, six J1005 and four J1008 samples were measured. About 250 mg of freeze-dried sediments were homogenized using a mortar and pastel and placed in acid-cleaned 50 mL centrifuge tubes. Sediments were digested using 40 mL of 1 mol/L Na_2CO_3 solution in an 80 °C water bath. The tubes were shaken very quickly every 20 minutes for complete digestion. After 3 hours of digestion, the tubes were dipped in cool water for 5 minutes to stop the chemical reaction and then centrifuged for 2 minutes at 4200 rpm. Subsamples of 1 mL were taken from the upper solvent. Tubes were returned to the 80 °C water bath after vortex and sonication (1 minute). The subsampling procedure was repeated at the 4 and 5 h our marks of digestion time.

The molybdate reagent and the reducing reagent were prepared before the molybdate blue measurement. About 4.0 g of ammonium paramolybdate and 12 mL of concentrated HCl were dissolved in DI water, with a total volume of 500 mL. This solvent was further diluted with DI water (2:5/v:v) to the make molybdate reagent (pH ~ 1.2). The reducing reagent was a mixture of metol-sulfite solution (6 g of anhydrous sodium sulfite and 10 g of metol in 500 mL DI water), saturated oxalic acid solution, 50% sulphuric acid solution and DI water (5:3:3:4/v:v:v:v).

200 µL of the aforementioned subsample was pipetted into a 30 mL acid-cleaned plastic bottle containing 7 mL of molybdate reagent and mixed immediately. After 20 min, 3 mL of reducing reagent were added to the bottle and mixed rapidly. The bottles were capped and left to sit in the laminar flow hood for more than 12 hours for complete reduction.

Finally, the absorbance of the solution was measured in a 1-cm cell with an Algilent Cary 60 UV-Vis spectrophotometer peaked at 812 nm. Two operational blanks that went through digestion and molybdate blue procedures were analyzed for each batch.

Text S2.

Data Processing and Evaluation

The weight percentage of biogenic silica was calculated as:

$$SiOpal\% = 112.4*F*(As-Ao)/M$$

where F is the slope resulted from standard calibration (F=2.763194); As and Ao refers to the absorbance of each subsample and operational blank, respectively; M stands for the weight of each sample in mg.

Percent biogenic opal was calculated as:

$$opal\% = 2.4* SiOpal\%$$

The "mineral correction" procedures were introduced to calibrate the contribution of mineral silicates. This continuous measurement requires a level of sophistication because subsampling is time sensitive and may result in possible mineral reprecipitation. During an ideal digestion, diatoms were quickly dissolved within 2 hours, while mineral silicates were slowly digested throughout the whole experiment.

A linear regression ($r^2>0.6$) was made for each sample based on the measured opal% of three subsamples versus digestion time, and the extrapolation to the intercept was taken as the corrected opal% for each sample (DeMaster, 1981). Corrected opal% show remarkable correlation ($r^2=0.98$) with 3-hour measured opal% for five Expedition 379T sites along the Chilean Margin (representing both open ocean and slope settings) (Figure S1, Table S1). It can be inferred that the contribution of mineral silicates is consistent for all samples under our digestion settings. Thus, the final opal% could be calculated as 3-hour measured opal% minus 0.3. A total of 14 duplicates was measured for the wet-alkaline digestion, yielding a standard error of 0.35%.

Prominent low values of magnetic susceptibility were found in certain intervals of J1002 and J1007. These intervals were thought to be affected by possible reworking or dissolution. Eight samples from J1007 and one sample from J1002 at these intervals were thought to have underestimated opal contents (Table S2).

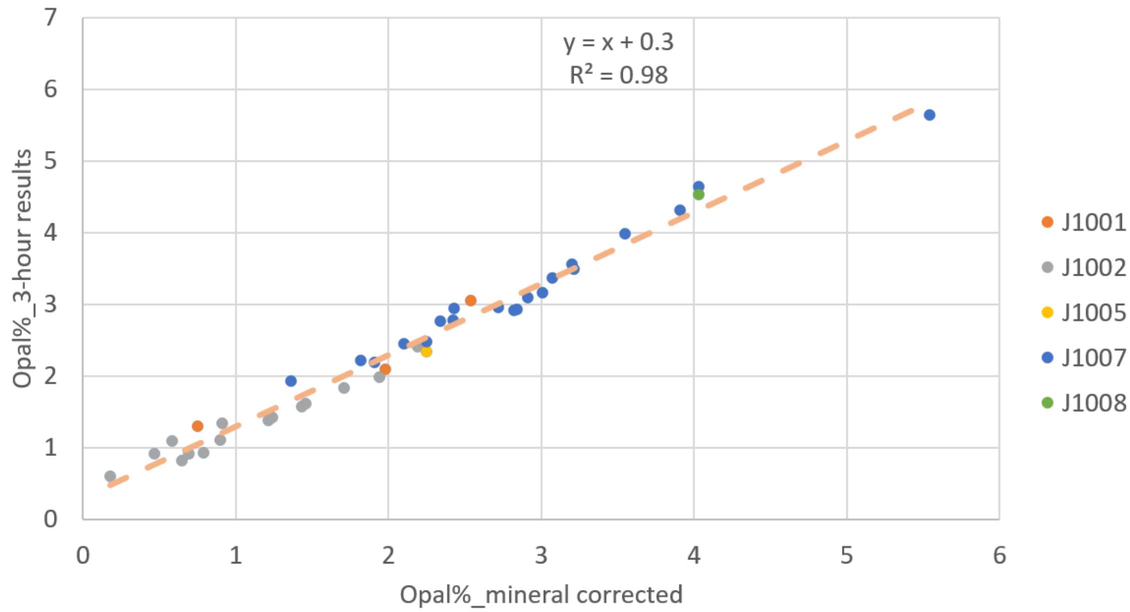

Figure S1. Mineral corrected opal% show remarkable correlation (r^2=0.98) with 3-hour measured opal% at five sites along the Chilean Margin.

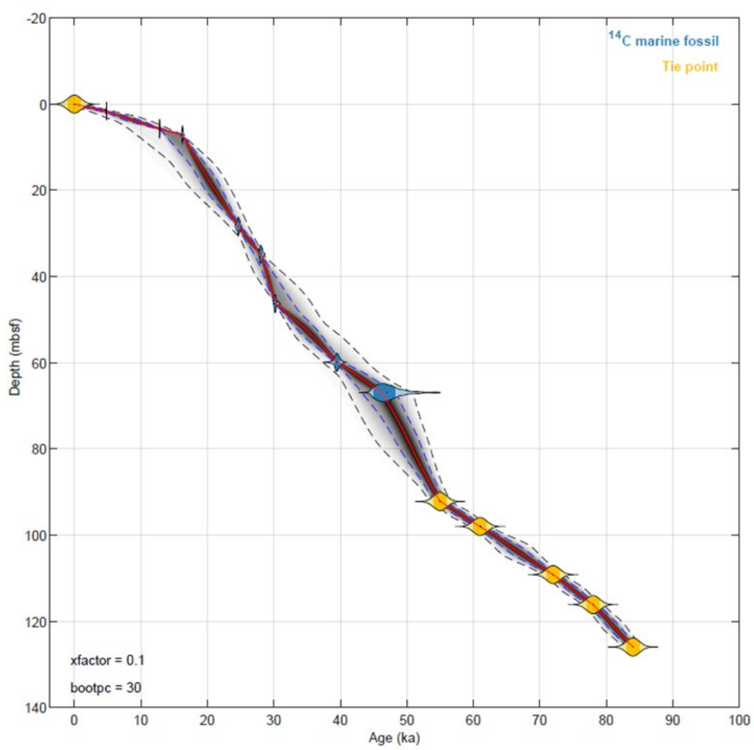

Figure S2. Depth-age relationship of Site J1002 from Undatable program (Lougheed et al., 2019). Yellow marks show the tie points of visual correlation between J1002 benthic *Uvigerina* spp. $\delta^{18}O$ and LR04 benthic stack (Lisiecki and Raymo, 2005). Blue marks are the ^{14}C ages derived from planktonic foraminifera (*Globigerina bulloides*).

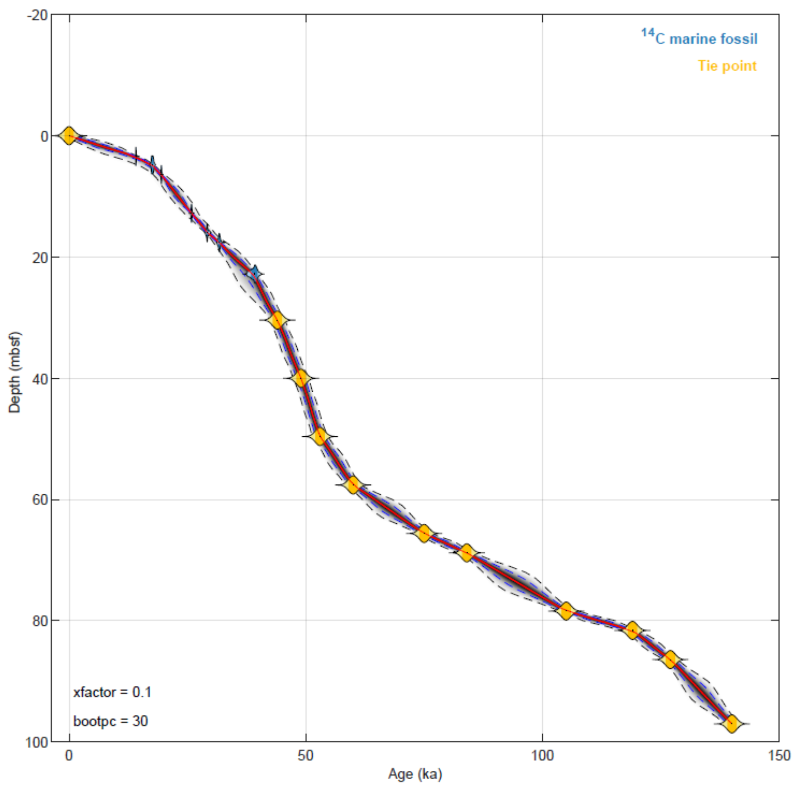

Figure S3. Depth-age relationship of Site J1007 from Undatable program (Lougheed et al., 2019). Yellow marks show the tie points of visual correlation between J1007 benthic *Uvigerina* spp. $\delta^{18}O$ and LR04 benthic stack (Lisiecki and Raymo, 2005). Blue marks are the ^{14}C ages derived from planktonic foraminifera (*Globigerina bulloides*).

Table S1. Mineral corrected opal% vs 3-hour measured opal%.

SITE	mineral corrected opal%	opal%_3-hour results
J1001	0.75	1.3
J1001	1.98	2.1
J1001	2.54	3.05
J1002	0.18	0.6
J1002	0.47	0.92
J1002	0.58	1.09
J1002	0.65	0.82
J1002	0.69	0.91
J1002	0.79	0.93
J1002	0.9	1.11
J1002	0.91	1.34
J1002	1.21	1.38
J1002	1.24	1.42
J1002	1.43	1.57
J1002	1.46	1.62

J1002	1.71	1.83
J1002	1.94	1.99
J1002	2.19	2.41
J1005	2.25	2.34
J1007	1.36	1.93
J1007	1.82	2.22
J1007	1.91	2.19
J1007	2.1	2.45
J1007	2.25	2.48
J1007	2.34	2.76
J1007	2.42	2.78
J1007	2.43	2.94
J1007	2.72	2.96
J1007	2.82	2.92
J1007	2.84	2.93
J1007	2.91	3.1
J1007	3.01	3.17
J1007	3.07	3.37
J1007	3.2	3.56
J1007	3.21	3.49
J1007	3.55	3.98
J1007	3.91	4.32
J1007	4.03	4.64
J1007	5.54	5.64
J1008	4.03	4.54

Table S2. Measured opal% for Site J1002 and J007.

Site	Depth	Age	GB	OPAL	notes
J1002	0.105	0.30	1.232	4.36	
J1002	1.605	4.48	1.262	2.11	
J1002	2.905	7.24	1.224	2.87	
J1002	4.305	9.98	1.207	2.61	
J1002	5.705	12.84	1.139	1.69	
J1002	7.105	15.98	1.123	1.07	
J1002	36.192	28.35	1.018	0.63	
J1002	43.194	29.69	1.003	0.36	
J1002	59.883	39.60	1.114	0.91	
J1002	61.303	40.92	1.05	0.7	
J1002	64.113	43.55	1.088	0.81	
J1002	92.216	55.12	1.199	1.45	
J1002	121.762	81.39	1.039	1.53	

J1002	124.482	83.04	1.12	1.04	
J1007	0.11	0.44	1.185	3.54	
J1007	6.409	19.37	1.169	2.8	
J1007	9.609	22.64	1.116	1.92	
J1007	11.209	24.25	1.108	1.89	
J1007	12.803	25.89	1.079	2.63	
J1007	14.393	27.61	1.126	4.34	
J1007	22.375	38.11	1.187	3.8	
J1007	25.606	40.64	1.162	3.81	
J1007	27.236	41.65	1.183	3.91	
J1007	33.599	45.72	1.189	4.9	
J1007	41.606	49.70	1.137	3.41	
J1007	43.206	50.38	1.186	4.34	
J1007	48.001	52.29	1.238	5.34	
J1007	49.605	53.11	1.177	5.35	
J1007	60.801	66.01	1.098	2.4	
J1007	67.197	79.48	1.121	2.87	
J1007	70.298	87.32	1.185	2.83	
J1007	72.003	91.02	1.129	2.77	
J1007	75.203	97.94	1.135	3.53	
J1007	81.596	118.31	1.186	3.65	
J1007	89.602	130.97	1.146	2.85	
J1007	99.979	143.95	1.224	3.74	
J1002	104.965	67.80	1.04	0.62	Data points with underestimated opal contents.
J1007	1.605	6.44	1.208	2.2	Data points with underestimated opal contents.
J1007	1.615	6.48	1.22	2.55	Data points with underestimated opal contents.
J1007	3.205	12.87	1.187	1.99	Data points with underestimated opal contents.
J1007	52.005	55.16	1.243	3.03	Data points with underestimated opal contents.
J1007	52.805	55.84	1.25	3.97	Data points with underestimated opal contents.
J1007	53.605	56.49	1.253	2.53	Data points with underestimated opal contents.
J1007	54.405	57.15	1.215	1.98	Data points with underestimated opal contents.
J1007	93.838	136.04	1.207	2.74	Data points with underestimated opal contents.

Table S3. Age control points for J1002 and J1007.

Site	Depth (mbsf)	Uncrorrected Age (yr)	Age error (yr)	Date type	Calibration
J1002	0	0		core-top	None
J1002	1.605	4245	25	14C_age	IntCal20
J1002	5.705	10925	40	14C_age	IntCal20
J1002	7.105	13475	45	14C_age	IntCal20
J1002	28.305	20490	90	14C_age	IntCal20
J1002	34.792	23950	110	14C_age	IntCal20
J1002	46.284	26000	160	14C_age	IntCal20
J1002	59.883	34310	370	14C_age	IntCal20
J1002	66.918	44000	1600	14C_age	IntCal20
J1002	92.22	55000		tie point	None
J1002	97.99	61000		tie point	None
J1002	109.16	72000		tie point	None
J1002	116.12	78000		tie point	None
J1002	125.96	84000		tie point	None
J1007	0	0		core-top	None
J1007	3.41	12230	35	14C_age	IntCal20
J1007	4.797	14430	140	14C_age	IntCal20
J1007	6.409	16150	70	14C_age	IntCal20
J1007	12.79	21570	130	14C_age	IntCal20
J1007	15.99	24970	170	14C_age	IntCal20
J1007	17.583	27820	190	14C_age	IntCal20
J1007	22.765	34080	480	14C_age	IntCal20
J1007	30.408	44000		tie point	None
J1007	40.006	49000		tie point	None
J1007	49.605	53000		tie point	None
J1007	57.601	60000		tie point	None
J1007	65.602	75000		tie point	None
J1007	68.797	84000		tie point	None
J1007	78.399	105000		tie point	None
J1007	81.596	119000		tie point	None
J1007	86.4	127000		tie point	None
J1007	97.008	140000		tie point	None

Table S4. Measured C_{org}% for J1007.

Depth_CCSF_m	G/B	Corg%	
0.1	1.182	2.38	
0.11	1.185	2.02	
4.797	1.141	0.67	

6.409	1.169	0.76	
8.009	1.088	0.75	
9.609	1.116	0.8	
11.209	1.108	0.87	
12.803	1.079	0.74	
14.393	1.126	0.92	
16.003	1.133	1.11	
17.61	1.17	1.08	
19.21	1.163	1.06	
20.83	1.187	0.92	
22.375	1.187	0.99	
24.006	1.171	0.97	
25.606	1.162	1.19	
27.236	1.183	1.03	
28.808	1.161	0.9	
30.408	1.179	1	
32.008	1.192	1.09	
33.599	1.189	1.13	
35.199	1.166	0.71	
36.799	1.172	0.73	
38.399	1.141	0.76	
40.006	1.128	0.82	
41.606	1.137	0.92	
44.801	1.178	1	
46.401	1.165	1.24	
48.001	1.238	1.92	
49.605	1.177	1.63	
50.405	1.196	1.3	
51.205	1.216	2.19	
55.205	1.203	0.81	
56.001	1.236	0.75	
56.806	1.168	0.64	
57.601	1.172	0.73	
59.201	1.126	0.6	
60.801	1.098	0.64	
62.402	1.162	0.81	
64.002	1.187	0.73	
64.802	1.169	0.73	
65.602	1.151	0.67	
67.197	1.121	0.71	
68.797	1.093	0.6	
70.298	1.185	0.66	

72.003	1.129	0.69	
73.603	1.167	0.7	
74.303	1.168	0.66	
74.803	1.116	0.66	
75.203	1.135	0.7	
75.703	1.152	0.68	
76.204	1.172	0.68	
76.799	1.18	0.71	
78.399	1.147	0.71	
79.996	1.188	0.84	
80.501	1.265	0.94	
81.001	1.238	0.93	
81.596	1.186	0.8	
83.2	1.189	0.8	
84.8	1.186	0.7	
86.4	1.126	0.58	
87.86	1.171	0.68	
89.602	1.146	0.73	
92.202	1.178	0.97	
95.408	1.287	1.49	
97.008	1.214	0.64	
98.609	1.201	0.67	
99.979	1.224	0.93	
102.419	1.111	0.78	
103.413	1.136	0.6	
105.013	1.157	0.59	
106.613	1.124	0.53	
108.213	1.118	0.58	
111.454	1.084	0.61	
113.019	1.128	0.59	
114.615	1.217	1.15	
116.215	1.194	0.83	
117.815	1.234	0.9	
119.005	1.181	0.74	
1.605	1.208	1.72	Data points with underestimated opal contents.
1.615	1.22	1.86	Data points with underestimated opal contents.
3.205	1.187	1.16	Data points with underestimated opal contents.
52.005	1.243	1.27	Data points with underestimated opal contents.

52.805	1.25	1.43	Data points with underestimated opal contents.
53.605	1.253	1.25	Data points with underestimated opal contents.
54.405	1.215	0.9	Data points with underestimated opal contents.
93.838	1.207	0.89	Data points with underestimated opal contents.

Data Set S1. Site J1007 G/B, reconstructed opal%, linear sedimentation rate and opal mass accumulation rate data.

Data Set S2. Site J1002 G/B, reconstructed opal% data.

References

Conley, D. J., & Schelske, C. L. (2001). Biogenic Silica. In J. P. Smol, H. J. B. Birks, W. M. Last, R. S. Bradley, & K. Alverson (Eds.), Tracking Environmental Change Using Lake Sediments: Terrestrial, Algal, and Siliceous Indicators (pp. 281-293). Dordrecht: Springer Netherlands.

DeMaster, D. J., 1979. The marine budgets of silica and Ph.D. Dissertation, Yale University, 308 pp.

Lisiecki, L. E., & Raymo, M. E. (2005). A Pliocene-Pleistocene stack of 57 globally distributed benthic δ18O records. Paleoceanography, 20(1), n/a-n/a. doi:10.1029/2004pa001071

Lougheed, B. C., & Obrochta, S. P. (2019). A Rapid, Deterministic Age-Depth Modeling Routine for Geological Sequences With Inherent Depth Uncertainty. Paleoceanography and Paleoclimatology, 34(1), 122-133. doi:10.1029/2018pa003457

Mortlock, R. A., & Froelich, P. N. (1989). A simple method for the rapid determination of biogenic opal in pelagic marine sediments. Deep Sea Research Part A. Oceanographic Research Papers, 36(9), 1415-1426. doi:https://doi.org/10.1016/0198-0149(89)90092-7